Non–Debye relaxations in disordered ionic solids

Wolfgang Dieterich[(1)] and Philipp Maass[(1,2)]

[(1)] *Fachbereich Physik, Universität Konstanz, 78457 Konstanz, Germany*

[(2)] *Institut für Physik, Technische Universität Ilmenau, 98684 Ilmenau, Germany*

(January 8, 2002)

Abstract

Motions of charged defects in ionic solids, including glassy ionic conductors, defective crystals and composite materials, imply slow relaxation processes, which are observable within a wide range of timescales larger than microscopic (vibrational) times. These processes manifest themselves in numerous dynamical probes, like ac–conductivity, nuclear spin–relaxation, quasielastic neutron scattering and mechanical relaxation. The present theoretical understanding of the corresponding response functions is reviewed. Stochastic models based on ion hopping are the most natural approach for systems with structural disorder on microscopic length scales, but more coarse–grained, phenomenological schemes are addressed as well. Macroscopically inhomogeneous systems and interfacial problems are modeled by random impedance networks.

Generally, non–exponential relaxation gets enhanced when Coulomb interactions between ions are taken into account. This is demonstrated by large–scale Monte Carlo simulations of disordered lattice gases for ion diffusion and is supported further by new results on random dipolar systems in the context of the "nearly constant dielectric loss response".

1 Introduction

The understanding of mechanisms of atomic migration through solids is of fundamental importance in many branches of materials science. Details of the migration process at different length– and timescales can be studied by various experimental techniques like tracer diffusion, electrical dc– and ac–conductivity, nuclear magnetic resonance, mechanical relaxation, ultrasonic attenuation and neutron scattering. In solid electrolyte materials, characterized by long–range ionic transport, numerous

measurements have revealed rich dynamical behavior [1, 2], showing that a simple random-walk picture of the ionic motion with Gaussian statistics is inappropriate. Indeed, the dynamics are characterized by a subdiffusive motion on intermediate time scales and by an associated non–exponential temporal decay of the relevant relaxation or correlation functions. One reason for the strange dynamics is the intrinsic structural disorder, caused by a broad distribution of jump probabilities. A second reason are collective motions due to ion–ion interactions, which consist of short–range chemical interactions and long–range electrostatic interactions. The latter may be non–negligible even in dilute samples.

Even in comparatively simple materials like substitutionally disordered crystals the defect dynamics can be quite unexpected. As an example, consider the case of monovalent salts doped with divalent cations, where charge transport is dominated by a vacancy mechanism. Over a wide frequency–range, their ac–conductivity increases nearly linearly with frequency, $\sigma'(\omega) \simeq A(T)\,\omega$, with an "intensity" $A(T)$ that depends only weakly on temperature, provided the temperature is near or below room temperature. For random defect motion with Gaussian statistics, a conductivity being independent of frequency would rather be expected. Since $\chi''(\omega) \propto \sigma'(\omega)/\omega$, a behavior $\sigma'(\omega) \propto \omega$ is equivalent to a frequency–independent dielectric loss. In fact, this "nearly constant loss" (NCL) behavior seems to be "universally" observed in disordered systems at high frequencies and/or low temperatures [4–6].

More complex systems, such as glassy and polymeric ion conductors are a subject of continuing research both from the structural and the dynamic point of view. In the network glasses, e. g. in alkali–doped silicate or borate glasses, ions diffuse in a topologically disordered network. The coupling of the ionic motions to the network degrees of freedom and the interactions with the counterions are major issues in explaining peculiarities in their transport properties. These include anomalous composition–dependent dc–transport properties and Haven ratios in single–ion glasses [7] and the mixed–alkali effect in glasses with two species of migrating ions [8]. These stoichiometric effects, however, will not be our major focus here. Rather we will concentrate on the dispersive transport properties.

The frequency–dispersion of the dynamic conductivity in these complex materials follows a common pattern. Above some cross–over frequency $\omega_\sigma(T)$ it passes from the thermally activated dc–plateau $\sigma(\omega) \simeq \sigma_{\rm dc}(T)$, with $\sigma_{\rm dc}(T) \propto \omega_\sigma(T)$, to a regime

where

$$\sigma'(\omega) \propto \omega^{n_\sigma} \tag{1}$$

with exponents $n_\sigma \sim 0.6$ to 0.7 (the so–called Jonscher–type response [9, 10]). At even higher frequencies, $\omega > \omega_{\rm NCL}(T) \gg \omega_\sigma(T)$ up to about 100 GHz, NCL–behavior is recovered. Typically, for temperatures $T \lesssim 10^2$ K, $\sigma_{\rm dc}$ and even $\omega_{\rm NCL}(T)$ become too small to be observable so that the NCL–response dominates the spectrum and extends over many orders of magnitude [4]. It is worth to note that the distinction between the Jonscher regime and NCL regime is often not very sharp when considering the spectrum at a fixed temperature: One may describe the dispersive part of a conductivity isotherm also by a slowly increasing exponent $n(\omega)$ that at very high ω becomes close to one. For a clear distinction it is preferable to look at the conductivity in the (ω, T)-plane: In the Jonscher regime at small ω and high T the conductivity is thermally activated, while in the NCL regime at large ω and low T its temperature dependence is very weak.

Albeit cross-correlations between different ions are important, the basic mechanisms governing the electrical response can essentially be traced back to the motion of single ions, i.e. the time–dependent mean–square displacement $\langle r^2(t)\rangle$ of a tracer ion. This does not mean, however, that ion-ion interactions can be neglected, since they strongly affect $\langle r^2(t)\rangle$. Moreover, the basic qualitative behavior of $\langle r^2(t)\rangle$ is reflected also in other dynamical probes. It is not surprising therefore, that the common features characterizing the conductivity have a counterpart e.g. in nuclear spin relaxation (NSR). On the low–temperature (high–frequency) side of the maximum in the NSR–rate T_1^{-1}, the spectral function is non–Lorentzian such that [11]

$$T_1^{-1}(\omega) \propto \omega^{n_{SLR}-2} \tag{2}$$

with an exponent $n_{SLR} > 0$. The approximate relationship

$$k_{\rm B}T\sigma(\omega) \propto \frac{\omega^2}{T_1(\omega)} \tag{3}$$

suggests that in the NCL–regime the effective exponent n_{SLR} approaches unity. Mechanical relaxation experiments are qualitatively described by a frequency–dependent modulus

$$N''(\omega) \propto \frac{k_{\rm B}T\sigma(\omega)}{\omega} \tag{4}$$

Power–law dependencies of $N''(\omega)$ as well as non–Lorentzian line shapes in quasi–elastic neutron scattering confirm the idea of slow relaxation and complex dynamics as an intrinsic property of ion–conducting glasses.

So far we considered ion diffusion as a bulk property. Besides this, a variety of heterogeneous (macroscopically disordered) materials are known where interfacial transport dominates. Much studied examples are composite ionic conductors with heterogeneities on length scales of 1μm [12]. A somewhat analogous situation on much smaller length scales occurs in nanocrystalline conductors consisting of essentially insulating nano–particles and strongly disordered, highly conducting regions in between [13].

Finally, we address diffusion across interfaces as a problem of prime importance with respect to the performance of electrochemical cells. Interfacial roughness can lead to anomalous behavior in the dynamical impedance $Z(\omega)$, again in the form of power–laws, $Z''(\omega) \simeq \omega^{-\eta}$. In this case the exponent η depends on the degree of roughness of the interface [14].

The primary aim of theories in this area is to understand the essential mechanisms of these "quasi–universal" patterns of behavior, observable in many different substances. Appropriate models need to introduce some coarse–graining, which makes them independent of many details in the microscopic structure and chemical bounding. However, in contrast to a purely phenomenological description, the models to be discussed in this paper do reflect the microscopic migration steps of ions, a specific local structure, and ion–ion interactions. To include all of these aspects it is most convenient to employ a stochastic lattice gas as a general frame. In that model, particles perform stochastic moves among sites of a discrete lattice. Naturally these lattice sites represent the set of interstitial sites preferred by the ions in a given material. During an elementary hop, affected by thermal activation, the ions have to surmount some saddle point energy, which depends on the specific atomic environment. Because of ion–ion interactions, the effective saddle point energy and hence the hopping probability contains a contribution depending on the configuration of nearby ions. Such effects are the essential ingredients in the description of many–particle hopping and structural disorder considered here.

In a more refined description, the lattice gas approach would still be useful. The lattice can then be regarded as a discretization of continuous space, with a mesh size significantly smaller than interatomic distances. Now, a realistic energy landscape resulting, for example, from molecular dynamics simulation, can be translated into discrete site energies. In this way, the capability of lattice Monte Carlo simulations in predicting the long–time dynamics is linked to microscopic structural information. At present, works on such "multi-scale" treatments are only at their beginning. Most

of our later discussion is therefore focused on the above–mentioned, more traditional interpretation of the lattice gas.

2 Common representations of experimental data

Different suggestions were made in the past to characterize the dielectric response of complex ionic conductors in the Jonscher regime. It is helpful to summarize some of these suggestions here for later reference. The perhaps simplest description is that suggested by Jonscher [9, 10] (sometimes, in solid state ionics, also attributed to Almond, Duncan and West [15]),

$$\hat{\sigma}(\omega) = \sigma_{\rm dc}(T)\{1 + [i\omega/\omega_\sigma(T)]^{n_\sigma}\} \tag{5}$$

with the Jonscher exponent $n_\sigma \simeq 0.6 - 0.7$, see eq. (1). It has been found that $\omega_\sigma(T)$ is proportional to the dc–conductivity, $\omega_\sigma(T) \propto \sigma_{\rm dc}(T)$, which implies that the activation energy E_{ac} in the dispersive regime is reduced relative to the dc activation energy $E_{\rm dc}$ by a factor $(1 - n_\sigma)$, i.e. $E_{ac} = (1 - n_\sigma)E_{\rm dc}$. Even more striking, Barton [16], Nakijama [17] and Namikawa [18] independently verified for many materials that

$$\omega_\sigma = p\frac{\sigma_{\rm dc}}{\Delta\epsilon}, \qquad \Delta\epsilon = \epsilon_{\rm s} - \epsilon_\infty \tag{6}$$

where p is a constant close to one, and $\Delta\epsilon$ is the dielectric strength, i.e. the difference between the static and high frequency dielectric constants $\epsilon_{\rm s}$ and ϵ_∞, respectively. Equation (6) is known as the BNN relation.

As already mentioned in the Introduction, the power law in (5) with a fixed exponent n is not a very accurate description when considering broad frequency regimes extending beyond 100 MHz at room temperature. More generally, one may therefore write

$$\hat{\sigma}(\omega) = \sigma_{\rm dc}\, f(\omega/\omega_\sigma(T)), \tag{7}$$

where f is a scaling function and $\omega_\sigma(T)$ is given by the BNN relation (6). Recently it was shown that this scaling ansatz gives a very good description for single ionic glasses [19, 20]. In particular it was observed that the form of the scaling function depends only very weakly on the ionic concentration and even only weakly on the specific glass composition. It thus resembles a "quasi–universality" of conductivity spectra of single ionic glasses, albeit differences in the spectra appear upon detailed inspection [21].

It has been argued in [22] that if scaling of the spectra occurs, it must be of the BNN type. To this end it was assumed that the scaling is valid strictly down to the lowest frequencies. Under this assumption one can consider the low frequency expansion of the conductivity, which then must be of the form $\hat{\sigma}(\omega)\sigma_{\rm dc} \sim 1 - iA\omega/\omega_{\rm dc}$ with A being real (since $\hat{\sigma}^\star(\omega) = \hat{\sigma}(-\omega)$). Accordingly, one would find $\hat{\epsilon}(\omega) - \epsilon_\infty = i\hat{\sigma}(\omega)/\epsilon_0\omega \sim i\sigma_{\rm dc}/\epsilon_0\omega + A\sigma_{\rm dc}/\epsilon_0\omega_\sigma$ for $\omega \to 0$, which implies $\Delta\epsilon = A\sigma_{\rm dc}/\epsilon_0\omega_\sigma$, i.e. the BNN relation.

However, the scaling in physical systems has typically to be understood in some limiting sense. It is well possible that a linear behavior of $\tilde{\sigma}(z,T)$ for small z is not in contradiction with the existence of a scaling function whose characteristic frequency is not connected to the low-frequency expansion. For example, one can have $\hat{\sigma}(\omega)/\sigma_{\rm dc} \sim 1 - iA\omega$ for $\omega \ll \omega_0(T)$, while $\hat{\sigma}(\omega)/\sigma_{\rm dc} \sim f(\omega/\omega_\sigma(T))$ for $\omega \gg \omega_0(T)$, where $\omega_0(T)$ is a cutoff frequency specifying the validity of the low-frequency expansion (which e.g. can be defined precisely by comparing the second term in this expansion with the first term). If now $\omega_0(T)/\omega_\sigma(T) \to 0$ for $T \to 0$, then the region $\omega \ll \omega_0(T)$ becomes irrelevant on the scale $\omega_\sigma(T)$ for low T. When one sets $\omega = u\,\omega_0$ with u fixed, then always $\lim_{T\to 0} f(u\,\omega_0(T)/\omega_\sigma(T)) = f(0) = 1$. For experiments (where always $T > 0$) this means that the part $\omega \ll \omega_0(T)$ of the spectrum practically disappears within the dc-plateau, when the spectrum is plotted on the frequency scale ω_σ (note in particular that ω_σ becomes very small for low T, so that ω_0 might become extremely small, i.e. the region $\omega \ll \omega_0(T)$ may not be resolvable at all).

An alternative way of representing data is by means of the electric modulus

$$\hat{M}(\omega) = \frac{1}{\hat{\epsilon}(\omega)}, \quad \hat{\epsilon}(\omega) - \epsilon_\infty = i\frac{\hat{\sigma}(\omega)}{\epsilon_0\omega}. \tag{8}$$

By linear response theory this modulus can be expressed in terms of a normalized relaxation function $\phi(t)$ with $\phi(0) = 1$, that describes the decay of an electric field $E(t)$ inside the sample after an external field is switched off, $E(t) = E(0)\phi(t)$. For materials with a finite dc-conductivity that relation is given by

$$\hat{M}(\omega) = -i\omega M_\infty \int_0^\infty dt\, \phi(t)\, e^{i\omega t}, \tag{9}$$

where $M_\infty = 1/\epsilon_\infty$. Equations (8,9) imply the "Maxwell relation" $\bar{\tau}^{-1} = \sigma_{\rm dc}/\epsilon_0\epsilon_\infty$, where $\bar{\tau} = \int \phi(t)\, dt$ is the mean relaxation time. We note that the Maxwell relation does not provide deeper insight into the BNN relation, since an assumption $\bar{\tau}^{-1} \propto \omega_\sigma$ would require justification (note that even a frequency-independent conductivity yields a peak in $-M''$ at a "characteristic frequency" $\sigma_{\rm dc}/\epsilon_0\epsilon_\infty$).

Reasonable fits of modulus spectra in the Jonscher regime are obtained by assuming a stretched exponential relaxation function

$$\phi(t) = \exp[-(t/\tau_{\mathrm{KWW}})^{\beta_{\mathrm{KWW}}}]\,, \tag{10}$$

often referred to as the Kohlrausch–Williams–Watts (KWW) function [23, 24]. As a rule of thumb, the conductivity exponent n_σ is related to β_{KWW} by $n_\sigma \simeq 1 - \beta_{\mathrm{KWW}}$ (for numerical relationships, see e.g. [25]). It should be noted that the KWW relaxation function has a non–analytic behavior at time $t = 0$, which, however, poses no real problem in practical situations, since the Jonscher regime terminates at large ω. A problem of practical importance, however, can arise from the fact that the modulus $\hat{M}(\omega)$ contains ϵ_∞ in a non–additive manner. This might complicate the interpretation of the spectra.

For completeness, let us finally mention that for complex materials with bound charges ($\sigma_{\mathrm{dc}} = 0$) dielectric spectra in the Jonscher regime are often represented by

$$\hat{\epsilon}(\omega) - \epsilon_\infty = \frac{\epsilon_{\mathrm{s}} - \epsilon_\infty}{(1 - (i\omega\tau)^{\alpha_{\mathrm{CC}}})^{\beta_{\mathrm{CD}}}} \tag{11}$$

which is a power–law–type generalization of the Debye behavior, the latter being recovered for $\alpha_{\mathrm{CC}} = \beta_{\mathrm{CD}} = 0$. The non–Debye behavior is accounted for by exponents α_{CC}, β_{CD} with values between zero and one, where different cases are distinguished according to various suggestions:

$\alpha_{\mathrm{CC}} \neq 0$	$\beta_{\mathrm{CD}} = 0$	Cole–Cole formula [26]
$\alpha_{\mathrm{CC}} = 0$	$\beta_{\mathrm{CD}} \neq 0$	Cole-Davidson formula [27]
$\alpha_{\mathrm{CC}} \neq 0$	$\beta_{\mathrm{CD}} \neq 0$	Havriliak-Negami formula [28]

Expressions of type (11) were used also to fit dielectric spectra of conducting materials by adding to these formulae the contribution $i\sigma_{\mathrm{dc}}/\epsilon_0\omega$ coming from the dc-conductivity. While the Cole–Cole formula yields symmetric arcs in a Cole–Cole plot of $\sigma'(\omega)$ versus $\sigma''(\omega)$, the arcs corresponding to the Cole–Davidson formula are skewed.

3 Single–Particle Approaches

3.1 Superposition of Debye processes

A non–Debye relaxation function $\phi(t)$ may in principle be obtained by a superposition of simple exponentials

$$\phi(t) = \int_0^\infty d\Gamma\, g(\Gamma)\, e^{-\Gamma t}. \tag{12}$$

The idea of such a concept is that the overall relaxation in a disordered structure originates from independent parallel Debye processes occurring in well–separated regions of the sample. The rates vary from region to region and have a weight ("spectral density") $g(\Gamma)$. Basically, however, this concept replaces the problem of explaining $\phi(t)$ by the problem of explaining $g(\tau)$. Hence no insight into the nature of the relaxation process is gained unless those separated regions are identified and $g(\Gamma)$ is explained by further modeling.

It is worth to note, nevertheless, that for the Kohlrausch function (10) the spectral density is

$$g(\Gamma) = \tau_{\rm KWW} L(\Gamma\tau_{\rm KWW})\,, \qquad L(u) = \int_{\epsilon-i\infty}^{\epsilon-i\infty} \frac{ds}{2\pi i}\, \exp(us - s^{\beta_{\rm KWW}})\,, \tag{13}$$

where $L(u)$ is the asymmetric Lévy stable law of index $(\beta_{\rm KWW}, 1)$ (see e.g. [29]). This stable law is a generalization of the Gaussian distribution for a sum of independent and identically distributed (iid) random variables with finite variance. In fact, L is the limit distribution of a sum of a large number N of iid positive random variables $\Gamma_i > 0$ with a probability density

$$\psi_\Gamma(\Gamma) \sim \Gamma^{-1-\beta_{\rm KWW}} \tag{14}$$

for $\Gamma \to \infty$ [30]. Note that for $0 < \beta_{\rm KWW} < 1$, $\psi_\Gamma(\Gamma)$ has no first moment, i.e. a mean relaxation rate does not exist. Let us mention also there should exist a cutoff of the power law (14) at large Γ when reaching vibrational frequencies, $\omega \gtrsim 100$GHz. This would lead to a modification of the Kohlrausch function at small times. Still, however, our understanding of the non–Debye relaxation is not improved as long as such power laws cannot be justified further.

3.2 Continuous–Time–Random–Walk (CTRW) Model

The CTRW model was set up by Montroll and Weiss [31] and further developed by Scher and Lax [32] to describe conductivity spectra in disordered systems. In that model, one particle performs jumps j with random displacements $\vec{a}_j$ at random times t_j, $j = 1, 2, \ldots$ The distribution of displacements has a finite first moment ($\langle \vec{a} \rangle = 0$ in the absence of a drift) and a finite second moment $\langle a^2 \rangle < \infty$. The times $\tau_j = t_j - t_{j-1}$ between successive jumps are randomly distributed according to some waiting time distribution (WTD) $\psi_\tau(\tau)$ and, in the separable CTRW model, the τ_j are uncorrelated with the $\vec{a}_j$.

The Laplace transform of the mean square displacement $\langle r^2(t) \rangle$ of the particle can then be expressed in terms of the Laplace transform $\tilde{\psi}_\tau(z) = \int_0^\infty \psi_\tau(\tau)\, e^{-z\tau}\, d\tau$ of the WTD [32],

$$\langle \tilde{r}^2(z) \rangle = \langle l^2 \rangle \frac{\tilde{\psi}_\tau(z)}{z[1 - \tilde{\psi}_\tau(z)]} \,. \tag{15}$$

Given the mean square displacement, the frequency-dependent diffusion coefficient is

$$\tilde{D}(z) = \frac{z^2}{6} \langle \tilde{r}^2(z) \rangle \,, \qquad \hat{D}(\omega) = \lim_{\epsilon \to +0} \tilde{D}(-i\omega + \epsilon) \,. \tag{16}$$

and the conductivity follows from the Nernst–Einstein relation,

$$\hat{\sigma}(\omega) = \frac{ne^2}{k_{\mathrm{B}} T} \hat{D}(\omega) \tag{17}$$

When assuming a power law decay $\psi_\tau(\tau) \sim \tau^{-2+n_\sigma}$ for large τ, it follows that $1 - \tilde{\psi}_\tau(z) \sim z^{1-n_\sigma}$ for small z and hence, from eqs. (15,16), $\sigma(\omega) \sim \omega^{n_\sigma}$ for small ω. More generally, one might map a given conductivity spectrum onto a WTD by (15,16).

However, apart from the question of explaining the origin the WTD one has to keep in mind that the formulae (15,16) do not apply to a stationary situation and hence cannot be used for ionic transport in solids, when the density of ions in phase space is in equilibrium. In a stationary situation, the WTD for the first jump of the particle is $h(\tau_1) \propto \int \psi_\tau(\tau_1 + \tau)\, d\tau$ due to the fact that the time instant of the jump preceeding the first jump is not known. Taking care of the WTD for this first jump leads to a frequency-independent conductivity $\sigma = ne^2 \langle l^2 \rangle / 6 k_{\mathrm{B}} T \langle \tau \rangle$, where $\langle \tau \rangle$ is the first moment of $\psi_\tau(\tau)$ [33]. That the CTRW in the stationary case yields a constant conductivity was first pointed out by Tunaley [34] for the separable CTRW. A thorough discussion including generalized CTRW's can be found in [35].

Physically, the result is not surprising, since the CTRW model for the stationary situation does not generate velocity correlations (correlations between the directions of the jumps). It hence yields a mean square displacement growing strictly linearly with time, corresponding to a frequency-independent conductivity.

3.3 Random Barrier Models

A picture often employed for describing transport in disordered materials is the jump motion of a particle in a random energy landscape. A particular simple model is the random barrier model (RBM), where iid random variables $V_{i,j} > 0$ are assigned to the bonds (i, j) of a lattice with spacing a, while the lattice sites are energetically equivalent. A particle performs a random walk in this lattice with jump rates

$$w_{i,j} = \nu \exp(-V_{i,j}/k_{\mathrm{B}}T) \tag{18}$$

where ν is an attempt frequency. The probability $p_i(t)$ to find the particle at site i at time t obeys the master equation

$$\frac{dp_i}{dt} = \sum_{j\mathrm{NN}i} w_{i,j}[p_j(t) - p_i(t)]\,, \qquad p_i(0) = \delta_{i,0}\,, \tag{19}$$

where the sum runs over all nearest neighbors (NN) of site i.

To calculate the thermally and disorder averaged mean square displacement $\langle r^2(t)\rangle$ of the particle, various approximation schemes were developed. For smooth distributions $\psi_V(V)$, a powerful tool is the effective medium approximation (EMA) [36, 37], or its "lattice variant", the coherent potential approximation (CPA) [38], and their various generalizations [39–43]. The idea of the EMA is to replace the random walk in the disordered environments by a random walk in an ordered effective medium, where the time correlations induced by the disorder are accounted for by a memory function $\gamma(t)$. The master equation in the associated effective medium thus reads

$$\frac{dp_i^{\mathrm{EMA}}}{dt} = \sum_{j\mathrm{NN}i} \int_0^t dt'\, \gamma(t-t')\,[p_j^{\mathrm{EMA}}(t') - p_i^{\mathrm{EMA}}(t')]\,, \qquad p_i^{\mathrm{EMA}}(0) = \delta_{i,0}\,, \tag{20}$$

or, in Laplace space,

$$z\tilde{p}_i^{\mathrm{EMA}} - \delta_{i,0} = \tilde{\gamma}(z) \sum_{j\mathrm{NN}i} [\tilde{p}_j^{\mathrm{EMA}}(z) - \tilde{p}_i^{\mathrm{EMA}}(z)]\,. \tag{21}$$

The memory function $\tilde{\gamma}(z)$ is determined by the requirement that on average the replacement of one bond in the effective lattice by a bond drawn from $\psi_V(V)$ has

no effect on the solution of eq. (19). The corresponding perturbation series can be summed up to all orders for the "single–bond EMA" and yields the following self-consistency equation for the memory function in a d-dimensional lattice

$$\left\langle \frac{\tilde{\gamma}(z) - w}{d\tilde{\gamma}(z) - [\tilde{\gamma}(z) - w][1 - zG_{00}(z)]} \right\rangle = 0\,. \tag{22}$$

Here $w = \nu \exp(-V/k_{\rm B}T)$, $\langle \ldots \rangle$ denotes an average over with respect to $\psi_V(V)$, and $G_{i,j}$ is the lattice Green function. For the d–dimensional cubic lattice,

$$G_{j,k}(z) = \int_{-\pi}^{\pi} \frac{d^d k}{(2\pi)^d} \frac{e^{i\vec{k}\cdot(\vec{a}_j - \vec{a}_k)}}{z + \tilde{\gamma}(z)\chi(\vec{k})}\,, \tag{23}$$

where $\chi(\vec{k}) = 2[d - \sum_{\mu=1}^{d} \cos k_\mu]$, and $\vec{a}_j$ denotes the position of site j. After solving eq. (22) for $\tilde{\gamma}(z)$, the mean square displacement of the particle is given by

$$\langle \tilde{r}^2(z) \rangle = \frac{\tilde{\gamma}(z)\, a^2}{z^2}\,, \tag{24}$$

and the conductivity follows from eq. (16).

The EMA is a good approximation of the conductivity at high frequencies but a serious problem is that it fails to predict the activation energy correctly. The reason for this failure is that the activation energy $E_{\rm dc}$ is determined by a percolation phenomenon [44]. At low temperatures the particle diffuses along the paths in the lattice where the barriers are lowest. The largest barrier $V_{\rm max}$ to be surmounted is given by the threshold for bond percolation [45],

$$\int_0^{V_{\rm max}} dV\, \psi_V(V) = p_c \tag{25}$$

and yields the activation energy $E_{\rm dc} = V_{\rm max}$.

In order to cope with the problem, Dyre and Schrøder suggested [46, 47] to truncate the distribution at $V_{\rm max}$, i.e. $\psi_V(V) \to \psi_{\rm trunc}(V) \propto \psi_V(V)\theta(V_{\rm max} - V)$ and to deal with the restricted geometry of the percolation path by using the EMA in $d = 1$. They called this method the "percolation path approximation" (PPA). Comparison with Monte–Carlo simulations [46] shows surprisingly good agreement in view of the fact that the complicated fractal topology of the percolation paths is ignored.

Recently a formal extension of the PPA was proposed [22] to account for the scaling features of ionic glasses in a quantitative manner (see Sec. 2). In this extension the dimension d in eqs. (22,23) is replaced by a "fractal dimension d_0" and then, in

the sprit of the PPA, the self–consistency equation is evaluated with the truncated distribution $\psi_{\rm trunc}(V)$ in order to determine $\tilde{\gamma}(z)$. This procedure, however, should be regarded only as a fitting method, since the Green function for diffusion on the percolation path is very different from (23) and has a much more complicated structure [48]. Irrespective of these various approximations for the RBM, it should be noted that the RBM in itself does not account for the variations of activation energies with ionic composition as they are found in experiment.

3.4 Random Site Energy Models

Somehow complementary to hopping models with random barriers one can consider random site energies. The variation of site energies is an important aspect, since the ions encounter quite different local environments in a disordered material. While the Coulomb potential of the immobile counterions gives rise to site energies being correlated over large distances, local structural inhomogeneities are typically of shorter range. In strongly disordered systems one may regard the local structural fluctuations to be dominant and consider a lattice model with uncorrelated site energies ϵ_i drawn from a distribution $\psi_\epsilon(\epsilon)$ as a starting point. By contrast to the barrier models it is important to take into account that two ions cannot occupy the same site. This is because the Fermi statistics hinders the ions to accumulate at the sites with lowest energies at low temperatures. In principle one is thus forced to treat a many particle problem, an issue considered further in section 5.

However, as it is known from electron hopping systems [49], for sufficiently low concentration of charge carriers one can map the many–body dynamics onto an effective one–particle dynamics. This is achieved by treating the site exclusion caused by the other particles in a mean–field type manner. The master equation analogous to eq. (19) then reads

$$\frac{dp_i}{dt} = \sum_{j{\rm NN}i} [w_{j,i}(1-f_i)p_j(t) - w_{i,j}(1-f_j)p_i(t)]\,, \qquad p_i(0) = \delta_{i,0}\,, \tag{26}$$

where $f_i = f(\epsilon_i) = \{\exp[(\epsilon_i - \mu)/k_{\rm B}T] + 1\}^{-1}$ is the Fermi equilibrium occupation. The jump rates $w_{i,j}$ from site i to j obey detailed balance, $w_{i,j}\exp(-\epsilon_i/k_{\rm B}T) = w_{j,i}\exp(-\epsilon_j/k_{\rm B}T)$, which ensures that $p_i^{eq} = f_i$ is a stationary solution of eq. (26). Note that this solution depends on the ionic concentration n via the chemical potential μ that is determined by the condition $\int d\epsilon\, \psi_\epsilon(\epsilon) f(\epsilon) = na^d$.

The effective one–particle master equation (26) is more complicated than the

corresponding one (19) for the random barrier model, since the jump rates $w_{i,j}(1-f_j)$ are not symmetric. In particular the standard EMA scheme discussed in the previous subsection cannot be applied. Formal extensions of the EMA to asymmetric rates were considered previously, in particular in the context of electron transport in amorphous semiconductors, see e.g. [50]. However, it is only recently that the reliability of the EMA in systems with site energy disorder has been investigated in detail. One of these studies focuses on the problem of quantum electron transport [51]. Another study deals with the problem of collective diffusion in classical hard-core lattice gases [52], when the transition rates depend on the initial site only.

Based on an EMA the problem given by eq. (26) was treated in [53, 54]. By introducing symmetrized jump rates $w^{\rm s}_{i,j} = w_{i,j}f_i(1-f_j) = w^{\rm s}_{j,i}$ and the rescaled probabilities $q_i(t) = p_i(t)/f_i$ eq. (26) can be rewritten as

$$f_i \frac{{\rm d}q_i(t)}{{\rm d}t} = \sum_{j{\rm NN}i} w^{\rm s}_{ij}[q_j(t) - q_i(t)]\,. \tag{27}$$

For a given energy ϵ_i of the final site, this master equation corresponds to a random walk with symmetric transition rates $w^{\rm s}_{i,j}$. Hence, analogous to the standard EMA, an ordered effective medium is introduced for each class of random walks ending at the same energy ϵ in time t. For this class of random walks the memory function $\tilde{\gamma}(z,\epsilon)$ depends on the final energy and is determined self-consistently by

$$\left\langle \frac{\tilde{\gamma}(z,\epsilon) - w^{\rm s}(\epsilon,\epsilon')}{d\tilde{\gamma}(z,\epsilon) - [\tilde{\gamma}(z,\epsilon) - w^{\rm s}(\epsilon,\epsilon')][1 - zf(\epsilon)G_{00}(z,\epsilon)]} \right\rangle_{\epsilon'} = 0\,, \tag{28}$$

where $\langle \ldots \rangle_{\epsilon'} = \int d\epsilon' \psi_\epsilon(\epsilon') \ldots$ denotes an average over the distribution $\psi_\epsilon(\epsilon')$ of site energies ϵ'. We note that the transition rates along two neighboring bonds in the real system are usually correlated, since they have one site energy in common (unless $w(\epsilon_i,\epsilon_j)$ depends on ϵ_i or ϵ_j only). These correlations are neglected in the single-bond EMA discussed here, but may be incorporated in extended cluster-type EMA versions.

The conductivity finally follows by averaging over the final energy ϵ, where each class of random walks with a terminal site energy ϵ is weighted by $f(\epsilon)$. One obtains for the conductivity [53, 55]

$$\tilde{\sigma}(z) = \frac{e^2}{k_{\rm B}Ta^d} \langle \tilde{\gamma}(z,\epsilon) \rangle_\epsilon \tag{29}$$

Equations (28,29) yield the correct high-frequency limit of the conductivity but fail in the zero-frequency limit for the same reasons as the EMA in the random barrier

model. Again one may correct this failure by invoking a critical percolation path argument [53]. We will not further discuss this issue here but note only that even with these corrections Monte–Carlo simulations do not give satisfying agreement with the EMA. The task to develop analytical tools to understand the dispersive transport in lattices with site energy disorder is still demanding.

Nevertheless, it is interesting to note that the EMA predicts a BNN scaling of conductivity spectra [54], where now also the dependence of the activation energy on the ionic concentration can be incorporated. With respect to simulations it was shown that a Fermi lattice gas model with Gaussian distributed site energies exhibits the BNN scaling features in the limit of low temperatures [56]. The master curve, however, is different from that obtained experimentally.

Similar to the approaches discussed in this and previous subsection, a general theory to describe non–Debye relaxations based on hopping models in disordered energy landscapes was developed by Hunt (for a review, see [57]). He uses extensions of the picture of hopping between two neighboring valleys ("pair–approximation", see the following section) to clusters of valleys, in order to treat the dispersive transport at high as well as intermediate frequencies. At lower frequencies, concepts from percolation theory were incorporated [58].

3.5 Asymmetric–Double–Well–Potential (ADWP) Model

A prominent model to understand the low–temperature anomalies of glasses is the system of independent two–level tunneling configurations [59, 60]. This model was used by Pollak and Pike [61] to describe a classical over-barrier hopping process and later further studied by Gilroy and Phillips [62], who termed it the asymmetric–double–well–potential (ADWP) model. It is now often invoked to explain the NCL behavior (cf. sec. 1). From a general point of view, the ADWP model can always be applied to classical hopping systems at high frequencies ("pair approximation").

In the model one considers two independent states of a double well potential that are separated by a barrier V and exhibit an energy difference Δ. If the two states refer to two positions of a charged particle with distance a, the dielectric response of identical ADWP configurations with number density n is calculated to be

$$\hat{\sigma}(\omega) = -\frac{ne^2a^2}{3k_\mathrm{B}T}\, p_1^\mathrm{eq} p_2^\mathrm{eq}\, \frac{i\omega}{1-i\omega\tau}\,, \qquad \tau = \frac{1}{w_1+w_2}\,, \tag{30}$$

where w_i is the jump rate out of state i and $p_i^\mathrm{eq} = w_i\tau$ is the equilibrium probability

of state i. Using $w_{1,2} = \nu \exp[-(V \pm \Delta/2)/k_{\rm B}T]$ in accordance with detailed balance, one finds

$$\hat{\sigma}(\omega) = -i\omega \frac{ne^2a^2}{12k_{\rm B}T} \frac{1}{1 - i\omega\tau} \frac{1}{\cosh^2(\Delta/k_{\rm B}T)}\,, \qquad \tau = \frac{\exp(V/k_{\rm B}T)}{2\nu\cosh(\Delta/k_{\rm B}T)}\,. \tag{31}$$

This corresponds to a Debye peak with a peak frequency $1/\tau$.

A smooth distribution $\psi_V(V)$ of barriers with support in some interval $(V_{\rm min}, V_{\rm max})$ gives rise to a broad distribution of τ values that varies smoothly in a regime $\exp(V_{\rm min}/k_{\rm B}T) \propto \tau_{\rm min} \ll \tau \ll \tau_{\rm max} \propto \exp(V_{\rm max}/k_{\rm B}T)$. For $1/\omega$ belonging to this regime, the averaging of $1/(1 - i\omega\tau)$ over V yields a function very weakly dependent on ω. This implies that the conductivity is approximately proportional to ω, corresponding to a NCL regime as discussed in the Introduction. By an additional averaging over the asymmetry parameter Δ one can furthermore tune the temperature dependence of the conductivity. In this way NCL regimes are successfully fitted [63].

3.6 Limitations of Single-Particle Models

In the single particle approaches discussed above the non-Debye relaxation behavior was associated with some distribution function ψ of parameters that characterize the disorder in the material. These distribution functions are rarely known from microscopic considerations. In any attempt to incorporate the effects of disorder one therefore has to make assumptions about the appropriate form of ψ. The physical significance of a chosen ψ can be supported, when its implications are found to be consistent with not only one but with a set of observables. Often it turns out that the main theoretical predictions are not very much affected by details in the form of ψ so that their validity is not strongly limited. On the other hand, in this case one cannot learn much from measurements of transport quantities about the specific character of the disorder in the material.

A more serious omission is the neglect of the ion-ion interactions. These interactions are typically strong and much larger than $k_{\rm B}T$ at room temperature. In the description of the effects of macroscopic heterogeneities in two- or multiphase systems, Coulomb interactions can be included most easily via random network models of impedances that are derived from the macroscopic Maxwell equations, see sec. 6. Such models are inapplicable to describe the microscopic ion dynamics in amorphous phases or strongly defective crystals with heterogeneities on atomic scales. Ion–ion

interactions can then manifest themselves in various ways. The simplest effect is a renormalization of parameters entering an effective single particle model. As interactions energies have to be compared to the thermal energy, the distribution function ψ will become temperature dependent.

Moreover, it is important to seek for a coherent explanation of the non-Debye behavior in different dynamical probes, where ion-ion interactions can play different roles. A well-known case is the distinction between the tracer diffusion and the charge diffusion constant, which in a many-particle system enters the Nernst-Einstein relation (17). In nuclear spin lattice relaxation it is the motion of pairs of ions that is probed and it is important that two ions do not like to become close to each other.

Problems with respect to the consistency in the ADWP model, when applied to the NCL response in glasses, are pointed out in sec. 5.2.

4 Phenomenological Theories

Various phenomenological approaches were proposed to describe ion transport in complex systems. In these approaches the ion-ion interactions are accounted for in an effective way so that one is again dealing with one-particle theories. The concepts leading to the basic transport equations, however, are borne out by interaction mediated correlation effects.

4.1 Defect Models

One of the earliest models to explain non–Debye behavior goes back to Glarum [64] who considered the overall relaxation to be caused by separated individual relaxation centers. By contrast to the superposition of Debye processes discussed in sec. 3.1, the centers have only one intrinsic relaxation rate γ_0. The non-Debye character of the overall relaxation is caused by an additional relaxation path that is followed once a defect arrives at a center. In this case the center is assumed to relax instantaneously. The defects diffuse through the material with a diffusion coefficient D_{def} and have a number density n_{def}. The relaxation function $\phi_{\mathrm{p}}(t)$ for the polarization of a center can then be written as

$$\phi_{\mathrm{p}}(t) = \exp(-\gamma_0 t)[1 - P(t)]\,, \tag{32}$$

where $[1 - P(t)]$ is the probability that no defect arrives at the center until time t. The dielectric function follows from

$$\frac{\hat{\epsilon}(\omega) - \epsilon_\infty}{\epsilon_s - \epsilon_\infty} = -\int_0^\infty dt\, \dot{\phi}_p(t)\, \exp(i\omega t)\,. \tag{33}$$

In the original version of the model, Glarum considered a one-dimensional system and assumed that it is sufficient to allow only the defect closest to a relaxation center to trigger the instantaneous relaxation. He showed that the dielectric response in this case resembles a Cole–Davidson behavior for $c \equiv \gamma_0/4Dn_{\rm def}^2 \gtrsim 1$ with an exponent $\beta_{\rm CD} \simeq c/(1+c)$. In the absence of an intrinsic relaxation process ($\gamma_0 = 0$) the Cole-Cole formula is recovered with $\beta_{\rm CC} = 1/2$.

Later Bordewijk [65] modified the Glarum model by allowing all defects to trigger a relaxation. Moreover, he considered the problem also in $d = 3$ dimensions, where the relaxation of a center is initiated once a defect enters a spherical region with radius R around the center position. For this more reasonable model one finds [65]

$$\phi_p(t) = \exp[-\gamma_1 t - (\gamma_2 t)^{1/2}]\,, \tag{34}$$

where $\gamma_1 = \gamma_0 + 64\pi D_{\rm def} R^4 n_{\rm def}^2$ and $\gamma_2 = 4\pi D_{\rm def} R n_{\rm def}$ [66]. For $\gamma_1 \ll \gamma_2$ (e.g. for $\gamma_0 = 0$ and $n_{\rm def} R^3 \ll 1$) the relaxation is dominated by a KWW function with exponent $\beta_{\rm KWW} = 1/2$.

Elliott and Owens [67] applied this model to ionic transport in glasses. To this end they considered the ion themselves to play the role of the defects by assuming that the dominant relaxation mechanism is the movement of an ion upon arrival of another ion in its neighborhood. The intrinsic relaxation process on the other hand refers to a more localized motion of an ion, as e.g. the motion from a stable to a metastable position in a given potential well. When calculating the dielectric function associated with eq. (34) from (33), one finds that for $\gamma_2 \gtrsim \gamma_1$, $\hat{\epsilon}(\omega)$ resembles a Cole–Davidson behavior, while for $\gamma_2 < \gamma_1$, the dielectric response is very similar to a Cole-Cole-form. Such models of relaxation controlled by ordinary defect diffusion were extended to diffusion on fractals in [68, 69] and to anomalous diffusion caused by long–time tails in waiting–time distributions [70, 71], see section 3.2.

4.2 Coupling Concept

The coupling concept developed by Ngai [72] is another prominent model for relaxations in complex systems. It has been applied to a huge variety of experiments,

including measurements of ionic transport quantities in disordered solids [2]. The coupling concept is based on the fact that the primitive relaxation of a microscopic unit at short times $t \ll t_c$ can be considered to be independent of the other species, while at larger times $t \gg t_c$ the interactions between the relaxing units have to be taken into account. The interactions require the primitive units to rearrange in a cooperative way to accomplish the relaxation.

The overall relaxation of some quantity Q (e.g. the polarization, electric field, magnetization) is characterized by a rate equation for the associated normalized relaxation function $\phi(t) = Q(t)/Q(0)$,

$$\frac{\mathrm{d}\phi}{\mathrm{d}t} = -W(t)\,\phi(t)\,, \tag{35}$$

where the time–dependent relaxation rate behaves as

$$W(t) \sim \begin{cases} W_0\,, & t \ll t_c \\ W_0\,(t/\tilde{t}_c)^{\beta_{\mathrm{KWW}}-1}\,, & t \gg t_c \end{cases} \tag{36}$$

The time $\tilde{t}_c$ equals t_c up to constants close to one and will be identified with t_c in the following.

In the original work [72] the power law in (36) was motivated by an infrared divergence of the excitation spectrum, which results from the Wigner distribution of energy eigenvalues associated with an Gaussian ensemble of random Hamilton matrices. Later attempts to justify eq. (36) in more detail refer to the chaotic nonlinear dynamics of many body systems [73–75]. The constant short–time relaxation rate W_0 is thermally activated, $W_0 = \nu \exp(-E_0/k_{\mathrm{B}}T)$, and the time t_c for the onset of the cooperative dynamics is assumed to be temperature independent. Experiments suggest t_c to be of the order of 1 ps.

Solving eq. (35) yields

$$\phi(t) \sim \begin{cases} \exp(-W_0 t)\,, & t \ll t_c \\ \exp[-(t/\tau_{\mathrm{KWW}})^{\beta_{\mathrm{KWW}}}]\,, & t \gg t_c \end{cases} \tag{37}$$

where

$$\tau_{\mathrm{KWW}} = \left[\frac{\beta_{\mathrm{KWW}}}{W_0 t_c}\right]^{1/\beta_{\mathrm{KWW}}} t_c\,. \tag{38}$$

Equation (38) relates, by continuity, the primitive relaxation time W_0^{-1} to the Kohlrausch relaxation time τ_{KWW}. Since t_c is temperature independent, eq. (38) is

very useful to correlate the parameters $\tau_{\rm KWW}$ and $\beta_{\rm KWW}$. In particular, W_0 can be extrapolated from Arrhenius plots of high–temperature data [76, 77].

With respect to temperature two situations can be distinguished: For large T, where $W_0 t_c \ll 1$, the decay of $\phi(t)$ is dominated by the simple exponential $\sim \exp(-W_0 t)$ and the stretched exponential is irrelevant. For low–temperatures by contrast, where $W_0 t_c \ll 1$, the exponential decay at short times contributes only a small amount to the overall relaxation, which is dominated by the Kohlrausch function. Accordingly, the coupling concept describes a crossover from a Debye behavior at high temperatures to a non–Debye relaxation at low temperatures with the relation (38) connecting these limiting behaviors.

4.3 Jump Relaxation Model

The jump relaxation model (JRM) was developed by Funke and coworkers [78] and attributes the dispersion in the conductivity to strong forward–backward jump correlations in the motion of an ion. These correlations have been considered in random walk theories [79] and their importance was early recognized for strongly correlated Coulomb systems [80]. The JRM is based on the following idea: After a hop of a "central ion" from an initially relaxed local configuration this ion is no longer in equilibrium with its surroundings. In order to stabilize the new position of the ion, the other ions its environment have to move. On the other hand, the ion can also jump back in order to (partially) relax the configuration after the jump.

The longer the ion stays at the new position after the jump, the smaller becomes the preference for a backward jump to occur. Denoting the probability $W(t)$ that no correlated [81] backward jump has occurred up to time t, the probability that a correlated backward jump occurs in the time interval $(t, t+\Delta t)$ is $[1-W(t+\Delta t)] - [1-W(t)] = -\dot{W}(t)\Delta t + O(\Delta t^2)$. Hence the backward jump rate is $-\dot{W}(t)$. The velocity correlation function of an ion may then be written as

$$\langle \vec{v}(t) \cdot \vec{v}(0) \rangle = \Gamma_0 \, a^2 \{ \delta(t) - [-\dot{W}(t)] \} \,, \tag{39}$$

where Γ_0 and a are the mean jump rate and mean jump distance, respectively. Since $\mathrm{d}^2\langle r^2(t)\rangle/\mathrm{d}t^2 = 2\langle \vec{v}(t)\cdot\vec{v}(0)\rangle$, and $\mathrm{d}\langle r^2(t)\rangle/\mathrm{d}t|_{t=0} = \Gamma_0 \, a^2$, integration of (39) from 0 to t yields [82]

$$W(t) = \frac{1}{\Gamma_0 \, a^2} \frac{\mathrm{d}}{\mathrm{d}t} \langle r^2(t) \rangle. \tag{40}$$

$W(t)$ can thus be considered as the normalized time derivative of the mean square displacement.

To quantify the stabilizing effect of the surrounding ions, a "mismatch function" $g(t)$ is defined that has the meaning of a normalized distance between the actual position of the central ion and the position at which it would be in local equilibrium with the other ions in its environment. The "stabilization rate" can then be thought to be proportional to $-\dot{g}(t)$ and the decrease of $W(t)$ occurs with this rate, i.e. $W(t+\Delta t) = W(t)\{1 - [-B \cdot g(t)]\Delta t + O(\Delta t^2)\}$, where B is a proportionality constant. This implies

$$\frac{\mathrm{d}W(t)}{\mathrm{d}t} = B\, W(t)\, \frac{\mathrm{d}g(t)}{\mathrm{d}t} \tag{41}$$

Once the function $g(t)$ is known, $W(t)$ can be calculated from (41) and in turn the conductivity is calculated via eqs. (40,16,17).

In recent years different levels of approximation for the function $g(t)$ have been employed. While in the early stages of the JRM an exponential function was considered, more sophisticated studies suggested $g(t)$ to decay in a non-exponential way [1].

Recently, an extension of the JRM was formulated, being called the Concept of Mismatch and Relaxation (CMR) [83]. In the CMR the time evolution of the mismatch function $g(t)$ is specified by the rate equation

$$-\frac{\mathrm{d}g(t)}{\mathrm{d}t} = A\, g(t)^K\, W(t)\,, \tag{42}$$

which for $K = 1$ can be reasoned by linear response type arguments. However, larger values of K are attributed to screening effects and give a better agreement with the experimental data. Comparison with experiments can be made by solving the two coupled eqs. (41,42) subject to the initial conditions $W(0) = g(0) = 1$. The two parameters A and B are connected to the limiting values of the conductivity: A is proportional to σ_∞, while $B = \ln[1/W(\infty)] = \ln(\sigma_\infty/\sigma_{\mathrm{dc}})$. By fitting measured conductivity spectra for different samples it was shown that $K = 2$ gives a very good description for high ionic concentrations and three-dimensional ion motion, while for lower concentrations of mobile ions and ion motion in lower dimensionalities, K turns out to be larger than two [83]. The overall approach accounts very well for the time–temperature scaling features of conductivity spectra of ionic glasses. The small changes of the master curves with the ionic concentration can be described by a proper choice of K.

5 Many–Particle Approach: Hopping with Ion–Ion Interactions

Various analytical as well as numerical approaches have been worked out to include interaction effects for hopping in regular lattice gases. Hard core systems have been treated by Green function techniques [84], while the path–probability method is particularly well–known for problems of stationary state hopping conduction in systems with short–range interactions.

An alternative way to describe tracer diffusion in lattice gases with short–range interactions is to use a kind of many–particle effective medium approximation [85–88]. The idea of this approach is that a neighboring site of a tracer particle becomes accessible within an initially unknown renewal time. The tracer diffusion coefficient D is then calculated by single–particle dynamic percolation theory. Using the result for D the initially unknown renewal time is determined self–consistently. The method has been extended to non–Poissonian renewal processes [89], which turned out to be particularly important for describing diffusion through polymer networks [90].

For particles interacting via long–range Coulombic interactions in regular lattices the dispersive transport properties and dynamic structure factors have been treated by the mode–coupling technique [91]. The strong non–Debye features of ionic motions in complex systems, however, require to go beyond regular lattices with equivalent sites and to take into some structural disorder. Such problems are no longer tractable by analytic means and one has to rely on simulation methods. Simulation studies of microscopic effects of ion–ion interactions were performed based on the lattice-gas Hamiltonian [92]

$$H(\{n\}) = \frac{e^2}{8\pi\epsilon_0} \sum_{i \neq j} \frac{n_i\, n_j}{|\vec{l_i} - \vec{l_j}|} + \sum_{i=1} \epsilon_i n_i \,, \tag{43}$$

where the sums run over all lattice sites, n_i are occupation numbers ($n_i = 1$ if lattice site i is occupied and zero else), and ϵ_i are site energies characterizing the disorder in the material. At most one ion is allowed to occupy a given lattice site, $n_i^2 = n_i$.

Metropolis jump rates are employed to specify the hopping dynamics of the ions, being explored by Monte–Carlo simulations. The ions are allowed to jump to vacant nearest neighbor sites with the rate $w = \nu \min(1, \exp(-\Delta H/k_{\rm B}T)$, where ΔH is the difference in energy after and before a jump according to (43), and ν is a bare hopping frequency. We choose ν^{-1} as the time unit. This corresponds to one Monte–

Carlo step (MCS), where on the average all particles have performed one jump trial. All quantities of interest are determined after equilibration of the system. Periodic boundary conditions are used and the long-range Coulomb interaction is taken into account by the Ewald summation technique. For further details we refer the reader to the original literature [93, 94].

Different types of disorder were investigated in order to check the robustness of the results. In the simpler models, one assumes the site energies to be uncorrelated. Two complimentary cases of the distribution $\psi_\epsilon(\epsilon)$ of site energies were considered in this situation [92, 94]:
(i) A percolative type of disorder, where only a fraction p of the lattice sites is accessible for the ions, with $p = 0.4$ well above the percolation threshold [98] ($p_c = 0.3117$ for the simple cubic lattice [45]). This type of disorder can formally be expressed by a distribution

$$\psi_\epsilon(\epsilon) = p\,\delta(\epsilon) + (1-p)\,\delta(\epsilon - \infty)\,, \qquad p = 0.4 > p_c\,. \tag{44a}$$

(ii) A smooth Gaussian distribution with zero mean and variance σ_ϵ^2 [92, 93]

$$\psi_\epsilon(\epsilon) = \frac{1}{(2\pi\sigma_\epsilon^2)^{1/2}}\,\exp\left(-\frac{\epsilon^2}{2\sigma_\epsilon^2}\right)\,. \tag{44b}$$

In a more realistic model the site energies were attributed to the Coulomb fields of immobile counterions [95–97]. These counterions are distributed randomly among the centers $\vec{R}_k$ of the cubic lattice cells. Denoting the fixed counterion occupation numbers of the cell centers by $\tilde{n}_k$, the site energies ϵ_i encountered by the mobile ions are

$$\epsilon_i = -\frac{e^2}{4\pi\epsilon_0}\sum_k \frac{\tilde{n}_k}{|\vec{l}_i - \vec{R}_k|}\,. \tag{44c}$$

Charge neutrality implies $\sum_k \tilde{n}_k = \sum_k n_k$. Clearly, the site energies are strongly correlated in this model.

5.1 Jonscher Regime

5.1.1 Tracer Diffusion

Figure 1 shows the time dependent diffusion coefficient [94]

$$D(t) = \frac{\langle r^2(t)\rangle}{6t} \tag{45}$$

of a tracer ion, *(a)* in the ordered lattice and *(b)* for the percolative type of disorder [eq. (44a)]. Data for different strengths of the Coulomb interaction are shown, specified in terms of the plasma parameter $\Gamma \equiv e^2/(4\pi\epsilon_0 r_s k_B T)$, where $r_s \equiv (3/4\pi n)^{1/3}$ is the half mean distance between the mobile ions. The concentration n of ions is $n = 0.01a^{-3}$.

For times $t \lesssim 1$ smaller than 1 MCS, $\langle r^2(t)\rangle$ is proportional to the total number of hops, which increases linearly with time and therefore $D(t)$ is constant, $D(t) = D_{\rm st}$. For $t > 1$, $D(t)$ decreases with t and finally approaches the long-time diffusion coefficient D_∞. In the ordered system, the decrease of $D(t)$ is comparatively weak, even at large plasma parameters Γ (low temperatures). In the disordered system, by contrast, $D(t)$ decreases over several orders of magnitude for large Γ. As shown by the solid lines in the figure, the data can be well fitted by

$$D(t) = D_\infty + (D_{\rm st} - D_\infty)\left(1 + \frac{t}{t_\times}\right)^{-n_{\rm D}} . \qquad (46)$$

For $\Gamma = 40$, 80 the cross-over time $t_\times$ to the long-time diffusivity becomes much larger than one. Hence a power-law regime $1 \ll t \ll t_\times$ can be identified in Fig. 1b, where $D(t) \sim t^{-n_{\rm D}}$ corresponding to a Jonscher type response. The exponent $n_{\rm D}$ is $n_{\rm D} \cong 0.63$ for $\Gamma = 40$ and $n_{\rm D} \cong 0.69$ for $\Gamma = 80$. This power law is connected with strong forward-backward correlations in the trajectory of a tracer particle. This has been shown by additional simulations of the mean–square displacement as a function of the number of performed hops [92], and is in accordance with the picture underlying the jump relaxation model, see sec. 4.3.

We can conclude from these results:

(i) Disorder is a necessary ingredient for understanding the Jonscher regime.

(ii) Ion-ion interactions strongly enhance the dispersive effects, so that also in systems with comparatively weak disorder a Jonscher type response is observed.

These features are not restricted to the percolative disorder considered in Fig. 1b but were found also for other types of disorder discussed in sec. 5 [eq. (44b)].

5.1.2 Frequency–dependent Conductivity

The time-dependence in the diffusion coefficient of a tagged particle, discussed so far, translates into a frequency-dependent diffusivity $\hat{D}(\omega)$, as given by eq. (16).

Of primary experimental relevance is the dynamic conductivity $\hat{\sigma}(\omega)$. For many–particle hopping, eq. (17) has to be corrected by a frequency–dependent Haven ratio $\hat{H}_{\rm R}(\omega) = ne^2\hat{D}(\omega)/k_{\rm B}T\hat{\sigma}(\omega)$, which expresses the strength of cross–correlations, i. e. the correlations in the motion of different particles. It turns out that $|\hat{H}_{\rm R}(\omega)| \leq 1$ is never far from unity so that in cases of strong dispersion the frequency-dependences of $\hat{D}(\omega)$ and $\hat{\sigma}(\omega)$ are essentially the same. In particular, $n_D \simeq n_\sigma$.

Particularly strong conductivity-dispersion between the dc- and high-frequency plateau is found for the counterion model, eq. (44c). Both real and imaginary parts of $\hat{\sigma}(\omega) = \sigma'(\omega) + i\sigma''(\omega)$ are plotted in Fig. 2 for a fixed concentration $na^3 = 0.03$ at various temperatures. The Coulomb interaction strength here is defined simply by $V = e^2/4\pi\epsilon_0 a$. Generally, the real part $\sigma'(\omega)$, see Fig. 2a, displays the features discussed in the introductory sections, suggesting a fit in terms of power laws. Closer analysis of the data for $V/k_{\rm B}T \gg 1$ and not too large frequencies yields exponents $n_\sigma \simeq 0.86$, which are somewhat larger, but similar to those observed experimentally. At larger frequencies, $\sigma'(\omega)$ appears to increase with even larger slope. This is indicative of the onset of an NCL-type regime, to be discussed in greater detail in sec. 5.2.

Figure 3 summarizes the occurrence of four distinct dynamical regimes in the counterion model. The respective crossover frequencies can be interpreted through characteristic times deduced from independent simulations of the mean-square displacement. Upon lowering the frequency, the plateau I terminates around $t = 1$ corresponding to 1 MCS or a time ν^{-1}. An NCL-type response II is observed as long as an ion has negligible chance to escape from a site next to a counterion. This criterion gets violated when $\langle r^2(\tau_{\rm NCL})\rangle = a^2$, and, indeed, one finds that $\omega_{\rm NCL} = 1/\tau_{\rm NCL}$. Finally, the crossover from the Jonscher regime III to the dc-plateau IV occurs, when an ion has a chance to leave the Coulomb basin connected with its (previous) counterion. This happens after a time $\tau_\sigma = \omega_\sigma^{-1}$, given by $\langle r^2(\tau_\sigma)\rangle = r_s^2$ ($r_s \equiv (3/4\pi n)^{1/3}$, cf. sec. 5.1.1). From these findings it is not surprising that $\sigma_{\rm dc}$ and ω_σ as a function of temperature are governed by the same activation energy $E_{\rm dc}$, which can be interpreted as an effective saddle point energy between adjacent counterions.

5.1.3 Spin–Lattice Relaxation

As discussed in the introduction, the non–Debye behavior seen in the conductivity is reflected also in other dynamical probes. The spin lattice relaxation rate $1/T_1$

is governed by the fluctuations of magnetic and electric fields at the nuclei of the mobile ions. In ionic conductors the main contributions to the fluctuations typically come from the magnetic dipole-dipole interaction between the ion nuclei and the interaction of the nuclear quadrupolar moment of one ion (with nuclear spin larger than 1/2) with the electric field gradient due to another ion. In both cases the relevant correlation functions $G^{(q)}(t)$ can be written as [99, 100],

$$G^{(q)}(t) = \frac{1}{N} \sum_{i \neq j}^{N} \langle F_{ij}^{(q)*}(t) F_{ij}^{(q)}(0) \rangle \,, \qquad q = 1, 2 \tag{47}$$

where $F_{ij}^{(q)}(t) = q(8\pi/15)^{1/2} Y_2^q(\Omega_{ij}(t))/r_{ij}^3(t)$ is the local field between the ions i and j. Y_2^q are the spherical harmonics, and Ω_{ij} and r_{ij} are the spherical coordinates of the vector $\vec{r}_{ij}$ pointing from ion i to ion j, with respect to the applied magnetic field. For an isotropic distribution of the ions one has $G^{(2)}(0) = 4G^{(1)}(0)$ [99].

Introducing the spectral densities $J^{(q)}(\omega)$ [99, 100] of the NMR correlation functions $G^{(q)}(t)$

$$J^{(q)}(\omega) = \int_{-\infty}^{\infty} G^{(q)}(t) e^{i\omega t} \, dt, \tag{48}$$

the spin lattice relaxation rate can be calculated from

$$\frac{1}{T_1} = C(J^{(1)}(\omega) + J^{(2)}(2\omega)) \,, \tag{49}$$

where $\omega = \gamma H$ is the Larmor frequency and the constant C in (49) depends on the nuclear properties of the mobile ions.

For an exponential decay $G^{(q)}(t) = G^{(q)}(t) \exp(-t/\tau)$ an Arrhenius plot of $\ln 1/T_1$ versus inverse temperature gives a symmetric curve that at the high temperature side ($\omega\tau \ll 1$) is frequency independent, while at the low temperature side ($\omega\tau \gg 1$), $1/T_1$ decreases as $\omega^{-2} = (\gamma H)^{-2}$ with increasing field H. This form is commonly referred to as the standard Bloembergen–Purcell–Pound (BPP) behavior.

Monte-Carlo simulations of the models introduced in sec. 5 show that Arrhenius plots of the spin lattice relaxation rate are indeed approximately symmetric *(i)* for ordered systems irrespective of the strength of the Coulomb interaction, and *(ii)* for disordered systems, when neglecting the Coulomb interaction. Again it is thus found [101] that the combined effect of disorder and Coulomb interaction reproduces the typical non-BPP-behavior seen in experiment, that means asymmetric Arrhenius plots of the spin lattice relaxation rates and an anomalous field dependence of $1/T_1$ on the low temperature side (cf. the discussion in sec. 1). A representative example

is shown in fig. 4 , where in part *(b)* the non-BPP behavior for a system with percolative type of disorder is displayed. To accomplish a reasonable comparison with experiment, the ratio of the characteristic Coulomb interaction energy $e^2/4\pi\epsilon_0 r_s$ to the bare structural energy barrier V_0 between the lattice sites was kept fixed, $(e^2/4\pi\epsilon_0 r_s)/V_0 = 5$ (for further details see [94]). Figures 4a and 4c show the BPP-like behavior for the corresponding ordered system and the disordered system when neglecting the Coulomb interaction, respectively.

5.1.4 Quasi–Elastic Neutron Scattering

The differential cross section measured in neutron scattering experiments is determined by the Fourier transforms of the van-Hove correlation function. Given an ion at the origin at zero time, the self part of this correlation function is the probability $P(\vec{r},t)$ for the same ion to be at position $\vec{r}$ at time t, while the distinct part is the probability for any ion to be at $\vec{r}$ at time t.

In the Jonscher regime $1 \ll t \ll t_\times$ (cf. sec. 5.1.1), the probability $P(\vec{r},t)$ strongly differs from a Gaussian. Nevertheless, studies in systems with percolative disorder [94] showed that a scaling ansatz

$$P(\vec{r},t) = P(\vec{0},t)\, h\left(\frac{r}{R(t)}\right) , \qquad R(t) \equiv \langle r^2(t)\rangle^{1/2} \tag{50}$$

with $P(\vec{0},t) \propto R(t)^{-3}$ can be made, where $R^2(t) \sim t^{1-n_{\rm D}}$. As shown in fig. 5, the scaling function $h(u)$ is found to decay as

$$h(u) \sim \exp(-C\, u^\mu) , \qquad u \gtrsim 1 . \tag{51}$$

Here C is a constant and $\mu \simeq 1.2$, i.e. one obtains a much slower decay compared to a Gaussian.

It is interesting that the value $\mu \simeq 1.2$ may be understood from a simple argument borrowed from [29]. Let us apply an external force f in the z-direction of the system. We then make the ansatz $P_f(\vec{r},t) \propto P(\vec{r},t)\exp(fz/k_{\rm B}T)$ to describe the change of $P(\vec{r},t)$ in the presence of the force. Accordingly, the drift $\langle z(t)\rangle_f$ of the ion is

$$\langle z(t)\rangle_f = \frac{\int d^3r\, z\, P(r,t)\, \exp(fz/k_{\rm B}T)}{\int d^3r\, P(r,t)\, \exp(fz/k_{\rm B}T)} . \tag{52}$$

For small times t, where $R(t)f \ll k_{\rm B}T$ (or $\langle z(t)\rangle_f f \ll k_{\rm B}T$) this implies

$$\langle z(t)\rangle_f \sim \frac{R^2(t)}{3k_{\rm B}T}\, f , \tag{53}$$

in agreement with the fluctuation–dissipation theorem.

For large times, however, the force always becomes strong ($\langle R(t)\rangle f \gtrsim k_{\rm B}T$) and the response will be nonlinear. Inserting eqs. (50,51) into eq. (52) and introducing cylinder coordinates $(\vec{\rho}, z)$ we obtain for the numerator in eq. (52)

$$\begin{aligned} & 2\pi P(\vec{0},t) \int dz\, z\, \exp\left(\frac{zf}{k_{\rm B}T}\right) \int_0^\infty d\rho\, \rho\, \exp\left[-c\,\left(\frac{\rho^2+z^2}{R^2(t)}\right)^{\mu/2}\right] \\ = \;& 2\pi P(\vec{0},t) \int dz\, z\, \exp\left(\frac{zf}{k_{\rm B}T}\right) \int_{z^2}^\infty dv\, \exp\left[-c\,\left(\frac{v}{R(t)}\right)^{\mu}\right]\,, \end{aligned}$$

and an equivalent expression for the denominator in eq. (52). Since the v-integral with the lower bound z^2 decreases as $\sim \exp\{-C[z/R(t)]^\mu\}$ for large z, we can use a saddle point approximation to perform the z-integration. The saddle $z_\star(t)$ is determined by

$$\left.\frac{\partial}{\partial z}\right|_{z_\star} \left[\frac{zf}{k_{\rm B}T} - C\,\left(\frac{z}{R(t)}\right)^{\mu}\right] = 0\,, \tag{54}$$

and yields, using $R^2(t) \sim t^{1-n_{\rm D}}$, the drift

$$\langle z(t)\rangle_f \sim z_\star(t) \sim t^{[(1-n_{\rm D})\mu]/[2(\mu-1)]}\, f^{1/(\mu-1)} \tag{55}$$

By requiring $\langle z(t)\rangle_f$ to be linear in t for large times, we finally obtain

$$\mu = \frac{2}{1+n_{\rm D}} \tag{56}$$

With $n_{\rm D} = 0.63$ for $\Gamma = 40$ and $n_{\rm D} = 0.69$ for $\Gamma = 80$ (cf. sec. 5.1.1), we find $\mu = 1.23$ and $\mu = 1.18$, respectively, in fair agreement with the value $\mu \simeq 1.2$ obtained from fig. 5. At present, however, it is not clear if this is a mere coincidence or if the ansatz for $P_f(\vec{r},t)$ and the consequences (55,56) can be substantiated by further analysis. To this end more detailed studies would be necessary and desirable.

It should be noted also that eq. (56) was earlier obtained in the context of random walks with long–range correlations (self–avoiding random walk, random walks on fractals [48]). In these systems the ansatz for $P_f(\vec{r},t)$ is better justified. In an interacting many–particle system a strong force leads to a redistribution of the ions in phase space compared to the equilibrium distribution in the absence of the force, and the use of $P(\vec{r},t)$ in the ansatz $P_f(\vec{r},t) \propto P(\vec{r},t)\exp(fz/k_{\rm B}T)$ is more questionable. Let us note finally that eqs. (55,56) would imply a nonlinear response $\langle z(t)\rangle_f \sim f^{(1+n_{\rm D})/(1-n_{\rm D})}$, which, however, should be difficult to observe experimentally.

The full form of $P(\vec{r},t)$ allows one to calculate the intermediate scattering function $S_{\rm inc}(\vec{k},t)$ and its Fourier transform, the incoherent structure factor $\hat{S}_{\rm inc}(\vec{k},\omega)$. For $kR(t) \ll 1$, in particular,

$$S_{\rm inc}(\vec{k},t) \simeq \exp\left(-\frac{k^2R^2(t)}{6}\right) . \tag{57}$$

In the Jonscher regime, where $R^2(t) \sim t^{1-n_{\rm D}}$, this leads to a slowing down of the decay compared to a Gaussian. As a consequence, broad quasi–elastic components appear in $\hat{S}_{\rm inc}(\vec{k},\omega)$ with an anomalous frequency dependence $\sim \omega^{n_{\rm D}-2}$ for $\omega \gtrsim (ka)^{2/(2-n_{\rm D})}$. This behavior is in qualitative agreement with experiments [1].

5.1.5 Mechanical Relaxation and Acoustic Attenuation

Generalized coherent dynamic structure factors of the subsystem of diffusing ions also pertain to mechanical relaxation and the attenuation of ultrasonic waves due to ion hopping. Let us first recall the well–known process of strain–induced relaxation of an isolated defect, subjected to a double–well potential (see sec. 3.5). Shear strains oscillating with frequency ω will modulate the asymmetry parameter Δ and thus drive the system out of equilibrium. Relaxation through activated hops over the barrier between the two wells gives rise to a Debye peak in the attenuation coefficient $\alpha(\omega)$ at the hopping frequency, and an associated change in sound velocity $\delta v(\omega)$ [102, 103].

The general mechanism for attenuation borne out in that two–site model can be taken over to a lattice gas description for a system of many interacting defects [104]. Suppose that in the presence of a particular sound mode with wave–vector $\vec{q}$, frequency ω and strain amplitude $u_{\vec{q}}$ the Hamiltonian (43) for an initially unperturbed lattice gas is changed into

$$H(\{n\},t) = H(\{n\}) + H'(\{n\},t) . \tag{58}$$

The perturbation

$$\begin{aligned} H'(\{n\},t) &= \sum_{\vec{l}} n_{\vec{l}}\,\delta\epsilon_{\vec{l}}(t) \\ &= A_{-q}u_q e^{-i\omega t} + c.c. \end{aligned} \tag{59}$$

with

$$A_q = \sum_{\vec{l}} g_{\vec{l}}\, n_{\vec{l}}\, e^{-i\vec{q}\vec{l}} \tag{60}$$

is caused by the modulation of site energies

$$\delta\epsilon_{\vec{l}}(t) = g_{\vec{l}} u_{\vec{q}} \exp[i(\vec{q}\vec{l} - \omega t)] \tag{61}$$

where $g_{\vec{l}}$ denotes the deformation potential of site $\vec{l}$. In a glass, all sites in general are non–equivalent, and the deformation potentials are subject to some distribution. In a crystal, due to the presence of defects, there exist at least certain groups of distinct sites with different $g_{\vec{l}}$'s. Hence we introduce the fluctuations $G_{\vec{l}} = g_{\vec{l}} - \bar{g}$, where $\bar{g}$ denotes the deformation potential averaged over all sites, so that $\sum_{\vec{l}} G_{\vec{l}} = 0$. In analogy with the two–site model described above, these parameters reflect the strain–induced site asymmetry. To simplify the discussion, we pass to the long wave–length limit, $\vec{q} \to 0$, where we can write $A_{\vec{q}\equiv 0} = \bar{g}N + A$. The first term contains the total number of ions, $N = \sum_{\vec{l}} n_{\vec{l}}$, which is a conserved quantity and need not be considered further, while the variable

$$A = \sum_{\vec{l}} G_{\vec{l}} n_{\vec{l}} \tag{62}$$

relates to the strain–induced redistribution of ions among the sites. To obtain the attenuation, it is most convenient to compute the power dissipated in the ionic system, which is equal to the energy loss per unit time of the acoustic mode. In terms of the generalized susceptibility $\chi(\omega)$ associated with the observable A,

$$\chi(\omega) = \beta(\langle A^2\rangle + i\omega \int_0^\infty dt\, e^{i\omega t}\langle A(t)A\rangle) \tag{63}$$

one finds

$$\alpha(\omega) = \frac{1}{\pi\rho v^3}\omega \,\mathrm{Im}\,\chi(\omega) \tag{64}$$

where $\beta = (k_\mathrm{B}T)^{-1}$, ρ is the mass density and v the unperturbed sound velocity. The associated change in sound velocity is given by

$$\delta v(\omega) = \frac{1}{\pi\rho v}(\chi(0) - \mathrm{Re}\,\chi(\omega)) \tag{65}$$

Debye expressions can be recovered by setting $\chi(\omega) = \chi(0)/(1 - i\omega\tau)$.

To proceed, we rewrite (64) as

$$\alpha(\omega) = \pi\frac{\Delta v}{v^2}\omega^2 s(\omega) \tag{66}$$

where $\Delta v = \delta v(\infty)$ is the difference between the high– and low–frequency sound velocity, and $s(\omega)$ is the normalized spectral function

$$s(\omega) = \frac{1}{2\pi}\int_{-\infty}^{\infty} dt\, e^{i\omega t}\langle A(t)A\rangle/\langle A^2\rangle \tag{67}$$

Without going into structural details of a given material, the expected qualitative behavior of $s(\omega)$ can be discussed as follows. Noting that $\sum G_{\vec{l}} = 0$, we argue that within few interatomic distances there are non–equivalent sites with positive and negative $G_{\vec{l}}$. The strained system can therefore equilibrate via purely local hops. Qualitatively, this idea is implemented most easily through a two–sublattice model: In a simple cubic lattice with spacing a, the two sublattices that correspond to a (1,1,1)–superstructure have deformation potentials G and $G' = -G$, so that $A = G \sum_l n_l \exp(-i\vec{k}^*\vec{l})$ with $\vec{k}^* = \pi(1,1,1)/a$. Equation (67) then becomes identical to the coherent dynamic structure factor normalized by the static structure factor, $s(\omega) = S(\vec{k}^*,\omega)/S(\vec{k}^*)$, and the total relaxational strength is determined by $\Delta v = (G^2/\pi\rho v k_{\rm B}T)S(k^*)$. The essence of these arguments is that, generally, the spectral function $s(\omega)$ in (66) will be related to the dynamic structure factor or a superposition of structure factors, taken at short wave–lengths reflecting the hopping distance between inequivalent sites with different deformation potentials.

To demonstrate the typical dynamics displayed by structure factors at short wave–lengths, numerical simulations for $S(k^*,\omega)$ were carried out within the counterion model, see eq. (44c) [104]. Results in the time–domain are plotted in fig. 6. After a fast initial drop one clearly observes a subsequent slower decay. A good representation of the data up to Monte Carlo times of the order $t \sim 10^4$ is achieved by writing

$$S(k^*,t)/S(k^*) \simeq (1-b)\exp(-t/\tau_0) + b\,\Phi(t) \tag{68}$$

where $\Phi(t) = \exp[-(t/\tau_{\rm KWW})^{\beta_{\rm KWW}}]$ is the Kohlrausch function. The KWW–exponent $\beta_{\rm KWW}$ decreases with temperature. At the lowest temperature in fig. 6, with $\beta V = 30$, one finds $\beta_{\rm KWW} \simeq 0.40$ and $b \simeq 0.48$, reflecting pronounced non–Debye relaxation. The relaxation time $\tau_{\rm KWW}$ follows an Arrhenius law, while the first, Debye–like term in (68) depends only weakly on temperature. Experimental attenuation spectra of ionic glasses were often analyzed in terms of the KWW relaxation function [105].

The above formalism immediately applies also to internal friction measurements, usually carried out at frequencies $\omega \lesssim 10^2\,s^{-1}$. Thereby, the mechanical modulus, see (4), is related to the spectral function (67) by $N''(\omega) \propto \omega s(\omega)$. Furthermore, an extension to a two–component lattice gas has been proposed as an attempt to describe the mixed–alkali effect in mechanical relaxation experiments [8].

5.2 NCL Regime

A nearly constant dielectric loss (NCL), as described in the Introduction, is an ubiquitous phenomenon in disordered materials, including ionic systems as well as polaronic conductors [3–5]. Yet its investigation has received fairly little attention up to now. The clearest evidence arises from several studies on low–conductivity materials up to megahertz frequencies and at temperatures below about 10^2 K, where the dc–conductivity $\sigma_{\rm dc}(T)$ becomes negligibly small. On the other hand, near room temperature, an NCL–response can still be observable, provided the measuring frequencies ω are sufficiently high ($\omega_{\rm NCL}(T) < \omega \sim 10^7$ to 10^{10} Hz). NCL–spectra in those two regimes seem to have different origins, but this question is not fully settled so far [106].

A collection of dielectric data for ionic conductors has been analyzed with respect to the NCL by Ngai [107]. Writing $\sigma'(\omega) \simeq A(T)\omega$, the dependence of the prefactor $A(T)$ on temperature, ion concentration and other materials parameters indicated that the physical origin of NCL–spectra should be sought in non–activated ionic displacements with amplitudes smaller than interatomic distances. Nowick et al. [108] proposed a similar picture of small–amplitude collective motions of cage ions relative to dopant ions in weakly doped crystals. Commonly, the ADWP–model (sec. 3.5) is used as a formal frame for the description of the NCL. However, as pointed out by Jain [106, 109], fits to experiment yield distribution functions $P(V, \Delta)$ which depend on temperature and ion concentration. This already raises the question as to the real physical significance of the effective barrier and asymmetry parameters V and Δ. Notice that fits of the ADWP–model to the room–temperature/high frequency NCL–response of ionic glasses require the distribution $P(V, \Delta)$ to extend to rather large values $V/k_{\rm B} \gtrsim 10^3$ K, significantly larger than assumed in the original works [61, 62].

A further difficulty with the ADWP–model arises from estimates of the strength of electric dipole–dipole interactions. Let us adopt for the moment the hypothesis that the loss spectrum of a given material is due to an ensemble of localized ADWP–like defects, distributed homogeneously in three–dimensional space with a number density $n = (4\pi r_s^3/3)^{-1}$. From eq. (30) the measured loss intensity provides an estimate for the quantity $n\,p^2$, where $p = ea$ denotes the magnitude of the electric dipole moment associated with the double well structure. Apart from a factor ϵ_∞, the same quantity $n\,p^2$ measures the strength of dipole–dipole interactions between the

defects, because these interactions decay with distance r as $V_{dip}(r) \simeq p^2/r^3$, so that $V_{dip}(r_s) \simeq p^2/r_s^3 \simeq c\,p^2$. However, for temperatures $k_{\rm B}T \lesssim V_{dip}(r_s)$ we will show by detailed model calculations that dipole–dipole interactions modify the dielectric loss spectra in a fundamental way. ADWP–parameters as given in [61] and [110] imply $n\,p^2/k_{\rm B} \gtrsim 10^2$ K, and hence suggest that the conventional ADWP–model without electrostatic interactions may become inconsistent at temperatures $T \lesssim 10^2$ K. Let us remark that additional long–range interactions of similar strength can originate from elastic deformations as, for example, in dipolar glass systems [111].

Before we turn to Monte Carlo simulations of a specific model, we demonstrate by an analytic argument that random dipolar interactions will quite generally lead to slow relaxation of the polarization. Clearly, a selected defect will interact most strongly with its closest neighbor. Suppose that within such a defect pair at distance r a barrier V_0/r^3 of the order $V_{dip}(r)$ has to be overcome in order to allow a relaxational step. The relaxation time is then given by

$$\tau(r) = \tau_0 e^{V_0/k_{\rm B}T} \tag{69}$$

and the relaxation function is determined by averaging $\exp[-t/\tau(r)]$ over all pairs,

$$C(t) = \text{const.} \int_0^\infty dr\, 4\pi n r^2\, \exp[-(4\pi n/3)r^3]\, \exp[-t/\tau(r)] \tag{70}$$

The weighting factor $4\pi n r^2 \exp[-(4\pi n/3)r^3]$ is the probability density that a defect has its closest neighbor at distance r. For $k_{\rm B}T < V_0/r_s^3$ and times $t > \tau_0 \exp[4\pi n V_0/3k_{\rm B}T]$, eq. (70) yields

$$C(t) \sim \frac{4\pi n}{3}\,\frac{V_0}{k_{\rm B}T}\,\frac{1}{\ln(t/\tau_0)} \tag{71}$$

This logarithmic decay in time converts to a logarithmic ω–dependence of the loss,

$$\chi''(\omega) \simeq \frac{1}{\ln^2(\omega\tau_0)} \tag{72}$$

which is "nearly constant" from an experimental viewpoint.

These arguments on the role of dipole–dipole interactions can be confirmed by Monte Carlo simulations of a dipolar lattice gas [112]. Select at random a fraction $na^3 \ll 1$ of unit cubes of a three–dimensional simple cubic lattice of size L with periodic boundary conditions. The midpoint of each selected cube carries a fixed negative charge $-q$, while a positive charge q ("cation") can undergo nearest–neighbor hops within the shell of eight binding sites surrounding the central charge.

Hopping probabilities, chosen according to the Metropolis algorithm, are based on Coulomb interactions among all charges. For sufficiently small n, dipole–dipole interactions will prevail; in that sense our model may be termed a "dipolar lattice gas", see fig. 7 for an illustration.

The complex dielectric susceptibility $\hat{\chi} = \chi' + i\chi''$ of that model is deduced in the standard way by simulating the correlation function of the total polarization; details are found in ref. [112]. Figure 8 shows plots of $\chi''(\omega)$ for $na^3 = 1/64$ and several temperatures, parameterized by $\Theta = 3k_{\mathrm{B}}T/4cp^2$. At higher temperatures, $\Theta \gtrsim 10$, the response is Debye–like, with a peak–frequency given by the average hopping rate. For lower Θ, however, $\chi''(\omega)$ develops an NCL–plateau, which at $\Theta = 0.8$ extends over at least three orders of magnitude. That dipolar lattice gas model therefore implies a mechanism for NCL–behavior. In comparison with (71) it is interesting to note that the "self"–part of the simulated correlation function indeed shows a logarithmic decay. Discussing the self–part seems sufficient since the "distinct"–part (containing cross–correlations between different defect centers) does not change the shape of the spectrum in a significant way, although its intensity even exceeds that of the self–part, cf. the discussion of Haven ratios in sec. 5.1.2.

Dynamic Monte Carlo simulations of this type can be regarded as a method for solving an underlying many–particle master equation. Hence the question arises, whether that master equation can also be treated analytically. An exact solution by straightforward diagonalization is limited to systems with a small number of defects, but already indicates "strange" dynamics [113]. An approximate analytic approach for larger systems, emphasizing the cooperativity of defect pairs, has recently been developed [96, 112]. That pair approximation, when applied to the present model, is able to qualitatively reproduce the simulated NCL–spectra. This analysis thus gives independent support for the ansatz made above that the pairs of closest dipoles dominate the relaxation spectrum.

6 Macroscopic Inhomogeneities: Complex Impedance Networks

So far we discussed various effects of microscopic disorder on the dynamic response of ionic systems, mostly by using the lattice gas approach. Different concepts are required in the description of heterogeneous systems showing disorder on macroscopic

length scales. More precisely, our concern are random mixtures of different phases, each phase being regarded as homogeneous from the point of view of macroscopic electromagnetism [114]. Electrical transport in such composite systems generally results both from bulk properties and from properties of the interfaces between the constitutive phases. As described below, interfacial effects can even become dominant. A closely related problem is the description of grain boundary effects in electroceramic materials [12]. Still another question of great practical importance is how to model the impedance of a given interface, including interfacial roughness and porosity [14, 115, 116, 139]. As is well known, the performance of electrochemical cells or electrical contacts in general, depends sensitively on such effects.

6.1 Disordered networks: Basic properties, percolation

The spatial distribution of the different components in a mixture defines a position–dependent complex dielectric permittivity $\hat{\epsilon}(\vec{r}, \omega)$. Theoretically, the problem is to solve for each frequency ω the equation $\vec{\nabla}(\hat{\epsilon}\vec{\nabla}\Phi) = 0$ for the electrostatic potential Φ under suitable boundary conditions. Using $\hat{\epsilon} = 1 + i\hat{\sigma}/\epsilon_0\omega$, where $\hat{\sigma}$ denotes the position–dependent complex conductivity that comprises all charge carriers, we rewrite this equation as [117]

$$\vec{\nabla}((\hat{\sigma} - i\epsilon_0\omega)\vec{\nabla}\Phi) = 0 \tag{73}$$

Clearly, in the case of random mixtures the primary task will be to calculate the configurationally averaged current, which determines the overall impedance. The most widely studied class of examples are random conductor–insulator mixtures, which constitute a paradigm for percolation [118, 119]. A mean–field description of a conductor–insulator transition controlled by percolation of the conducting component, is provided by effective medium theories (EMA), see sec. 3.3. In some applications the micro-geometry is such that one phase, e. g. the conducting phase, is always surrounded by the other (insulating) phase and never percolates. This situation is covered by the differential effective medium theory (DEMA) [120]. This theory has been used recently to work out the dc– and ac–response in a macroscopic model of polymer electrolytes [121].

For computational convenience, one often studies the discretized form of equation (73). On a simple–cubic lattice,

$$\sum_a g_{i+a,i}(\Phi_{i+a} - \Phi_i) = 0 \tag{74}$$

where the summation is over the nearest neighbor sites of site i [135, 141]. These equations can be interpreted as Kirchhoff's equations for the potentials Φ_i on the nodes of a network where nearest neighbor bonds $(i+a, i)$ carry complex conductance elements $g_{i+a,i} = \hat{\sigma}_{i+a,i} - i\epsilon_0\omega$. Most studies start out from a binary (AB) mixture, with "ideal" (dispersionless) conductances $\hat{\sigma}_\alpha(\omega) = \sigma_\alpha - i\epsilon_0(\epsilon_\alpha - 1)\omega$; $\alpha = A, B$ [122–124]. Here σ_α is given by the dc–conductivity of phase α and ϵ_α by its dielectric constant. To model a mixture without any correlations in the spatial arrangement of its components, conductance elements

$$g_\alpha(\omega) = \sigma_\alpha - i\omega\, C_\alpha; \qquad \alpha = A, B \tag{75}$$

are assigned randomly to the bonds of the network with probabilities p or $1-p$ for $\alpha = A$ or B, respectively. The equivalent circuit for one particular bond is a resistor with resistance $R_\alpha = 1/\sigma_\alpha$, in parallel with a capacitor with capacitance $C_\alpha = \epsilon_0\epsilon_\alpha$. Again, the task is to calculate an effective (homogeneous) bond conductance $g^{eff}(\omega)$, which determines the overall electrical response of the resistor/capacitor network. The case $\sigma_B = 0$ corresponds to a conductor/insulator mixture. Near the percolation threshold p_c and for $\omega \to 0$, $g^{eff}(\omega)$ takes the form [122]

$$g^{eff}(\omega) \simeq \sigma^{eff} - i\,\omega\, C^{eff} + O(\omega^2); \qquad p \neq p_c \tag{76}$$

The effective conductance $\sigma^{eff} = g^{eff}(0)$ and the effective capacitance

$$C^{eff} = -\lim_{\omega\to 0} \mathrm{Im}\, g^{eff}(\omega)/\omega \tag{77}$$

behave as $\sigma^{eff} \sim (p-p_c)^\mu$ for $p \to p_c^+$, and $C^{eff} \sim (p_c-p)^{-s}$ for $p \to p_c^-$, with critical exponents $\mu \simeq 1.99$ and $s \simeq 0.74$ in $d = 3$ dimensions [119], whereas $\mu = s \simeq 1.30$ in $d = 2$. These values originate from several theoretical techniques like the transfer matrix method [125], the renormalization group technique, exact enumeration and numerical simulation [126].

On the other hand, at the percolation threshold a non–analytic frequency–dependence

$$g^{eff}(\omega) \sim (i\omega)^u; \qquad p = p_c;\ \omega \to 0 \tag{78}$$

emerges. Standard scaling theory predicts that $u = \mu/(\mu+s)$. More generally, when the B–component is a "leaky dielectric" so that $0 < |g_B| \ll |g_A|$, then

$$g^{eff}(\omega) \simeq g_A^{1-u}(\omega) g_B^u(\omega) \tag{79}$$

at $p = p_c$. In the same limit, the effective capacitance at p_c develops a large, but finite peak [127],

$$C^{eff} \simeq C_B \left(\frac{\sigma_A}{\sigma_B}\right)^{1-u} \tag{80}$$

This equation explicitly illustrates that spatial variations of the real part of $g_{i+a,i}$, see equation (75), lead to an enhancement of the imaginary part of g^{eff} which is the effective capacitance C^{eff}, as a consequence of the build–up of polarization charges. Conversely, the capacitors in (74,75) give rise to a frequency–dependent real part Re $g^{eff}(\omega)$, as exemplified by equation (78).

A network with complex bond conductances $g_{i+a,i}(\omega) = \sigma_{i+a,i} - i\omega C$, where C is constant and $\sigma_{i+a,i}$ are independent real, continuous random variables, has been studied by Dyre [128]. In that model, the bond resistors proportional to $\exp(E/k_{\rm B}T)$ depend exponentially on a random activation energy E, which varies on energy scales large compared to $k_{\rm B}T$. In this extreme disorder limit [129], the EMA predicts a universal normalized conductivity $\tilde{\sigma} = (g^{eff}(\omega) + i\omega C)/g^{eff}(0)$, satisfying

$$\tilde{\sigma} \ln \tilde{\sigma} = i\tilde{\omega} \tag{81}$$

where $\tilde{\omega}$ is a suitable dimensionless frequency. This equation implies conductivity dispersion as described in previous sections.

To obtain quantitative estimates of the impedance of a heterogeneous medium, details of its microstructure have to be incorporated into the network equations (74). Two specific applications are outlined in the following.

6.2 Interfacial conductance in micro– and nano–composites

When insulating fine particles with sizes of about 0.1 to 1μm are dispersed in an ionically conducting medium, the overall conductivity can become enhanced. This surprising effect, discovered by Liang [130], arises from the formation of a defective, highly conducting layer following the boundaries between the conducting and the insulating phase [131]. Effectively, the system thus contains three phases and can be mapped onto a suitable three–component impedance network.

Figure 9 shows a two–dimensional illustration of such composites and a corresponding discretized model [132–134]. The random distribution of the insulating phase C (shaded areas) within the conducting phase B (white areas) defines a boundary which corresponds to a third, highly conducting component A (thick lines). In this way we arrive at a three–component, correlated bond percolation model. The conductance elements $g_\alpha = \sigma_\alpha - i\omega C$; $\alpha = A, B, C$; are chosen to have a constant capacitance C, and $\sigma_C = 0$; $\sigma_A/\sigma_B = \tau \gg 1$. Besides the ordinary conductor/insulator transition at a critical volume fraction p_c'' of the insulating C–phase, there exists a

second threshold p_c'' for interface percolation, i. e. percolation of A–bonds. Calculations of σ^{eff} as a function of composition compare favorably with experiment [135]. Critical ac–effects are expected near the onset of interfacial percolation, as shown by Blender et al. [127]. In particular, the effective capacitance C^{eff} develops a peak at p_c', whose height is given by eq. (80). The complex impedance diagram calculated from the model of fig. 9b at $p = p_c'$ is depicted in fig. 10 [142]. It turns out that the distorted semicircle in the (Z', Z'')–plane with $Z(\omega) = (g_{\text{eff}}(\omega))^{-1}$ is well approximated by (79). This equation entails a power–law dependence in the range $\omega_B \ll \omega \ll \tau\omega_B$ with $\omega_B = \sigma_B/C$, which reflects itself in a constant phase angle behavior near the origin where $Z''/Z' = \tan\delta$; $\delta = u\pi/2$.

The same ideas also hold for nanocrystalline conductors, where grain sizes are scaled down by a factor of about 50 in comparison with the dispersed ionic conductors described so far. In particular, Indris et al. [13] were able to demonstrate enhanced interfacial effects in nanocrystalline samples of $(1-x)\text{Li}_2\text{O} : \text{B}_2\text{O}_3$ relative to their microcrystalline counterparts, and to explain them by using the above theory.

6.3 Ac–response of fractal interfaces

The performance of any electrochemical device is controlled to a large extent by the properties of the respective electrolyte/electrode interfaces. A crucial parameter in any realistic electrode process is the geometry of the interface, which often is irregular. The problem of charge transport and diffusion across irregular interfaces therefore has stimulated intense research, with applications in many branches of heterogeneous chemistry [136] and biophysics [14].

A special process which can be analyzed successfully in terms of suitable network equations, is the double–layer impedance at a rough electrode. Several experiments have revealed an anomalous ac–impedance $Z(\omega)$, governed by power–laws in a certain frequency–range. Effective exponents were found to depend on the degree of roughness [137, 138]. A simplified, two–dimensional network model due to Blender et al. [139], which is adapted to these problems, is depicted in fig. 11. It ignores any detailed electrochemical process within the atomic layers in the vicinity of the interface but captures the essential geometrical effects on macroscopic scales. The electrolyte is represented by real bulk conductance elements σ_b, capacitance effects in the bulk being ignored, and is confined between a planar electrode S_0 and a rough

electrode S of the form of a hierarchical fractal. Successive stages N of the fractal boundary are generated as indicated in the figure, yielding a quadratic Koch curve with fractal dimension $d_f = \ln 8 / \ln 4$. At stage N, the system size (for fixed smallest length scale taken as unit length) is $L_N = 4^N$, the total length of the boundary S is $l_N = L_N^{d_f} = 8^N$. Each elementary segment of that boundary intersects one bond of the underlying square lattice. With these bonds we associate interface conductance elements σ_i. Their endpoints below the Koch curve are held at a fixed potential $\Phi = 0$, while $\Phi = \Phi_0 \propto e^{-i\omega t}$ on S_0. For an ideally blocking electrode we assume $\sigma_i = -i\omega C$, where C represents the double–layer capacitance per unit length.

Qualitatively, the overall N–dependent impedance $Z_N(\omega)$ will behave as follow. For very high frequencies such that $|\sigma_i| \gg \sigma_b$, we can neglect the resistances σ_i^{-1} so that the electrolyte effectively is in contact with a metallic electrode with potential $\Phi = 0$. In this infinite–frequency limit the tips of the electrode S which are closest to S_0 will carry most of the current, while the pores are shielded. Lowering the frequency, the equipotential lines will more and more be dragged in the pores. Ultimately, as $\omega \to 0$, we have $|\sigma_i| l_N \ll \sigma_b$. Then the full voltage Φ_0 drops to zero across the interface so that $Z_N(\omega) \simeq (\sigma_i \, l_N)^{-1}$. This discussion shows that the equipotential lines explore the interfacial geometry in way that depends on ω.

Before studying the discrete network of fig. 11 numerically, it is instructive to formulate the corresponding boundary value problem for the electrostatic potential $\Phi(\vec{r})$ in continuous space. Laplace' equation $\Delta\Phi = 0$ is supplemented by boundary conditions

$$\Phi(\vec{r}) = \Phi_0; \qquad \vec{r} \in S_0 \tag{82}$$

and

$$\sigma_b(\vec{n}\vec{\nabla}\Phi(\vec{r})) = \sigma_i \Phi(\vec{r}); \qquad \vec{r} \in S \tag{83}$$

The last equation with $\vec{n}$ a unit vector normal to S, exhibits two ways to express the normal current density j_n across S.

From a Green function representation of this problem [140] it is possible to derive a high–frequency expansion of the impedance

$$Z(\omega) = \Phi_0 \left[\int_S j_n \, d\sigma \right]^{-1} \tag{84}$$

The two leading terms are given by

$$\sigma_b Z(\omega) = a_0 - \frac{i}{x} a_1 + O(x^{-2}) \tag{85}$$

where $\sigma_i/\sigma_b = -ix$ with

$$x = \omega C/\sigma_b \tag{86}$$

One can show that

$$a_0 = \sigma_b \Phi_0 \left[\int_S j_n^\infty d\sigma \right]^{-1} \tag{87}$$

and

$$a_1 = \int_S (j_n^\infty)^2 d\sigma \left[\int_S j_n^\infty d\sigma \right]^{-2} \tag{88}$$

where

$$j_n^\infty = -\sigma_b (\vec{n} \vec{\nabla} \Phi^\infty(\vec{r})); \qquad \vec{r} \in S \tag{89}$$

In these equations $\Phi^\infty(\vec{r})$ denotes the electrostatic potential at infinite frequency, which instead of (83) satisfies $\Phi^\infty(\vec{r}) = 0$ for $\vec{r} \in S$. Notice that a_1 is the second moment of the "harmonic measure" $j_n^\infty (\int j_n^\infty d\sigma)^{-1}$ of the fractal boundary S, whose scaling with the system size L is determined by the multifractal exponent $\tau(2) \equiv \tau$,

$$a_1 \sim L^{-\tau} \tag{90}$$

It turns out that the first–order expansion (85) together with (90) greatly facilitates the interpretation of the subsequent numerical analysis. Clearly, the imaginary part $\mathrm{Im}\, Z_N$ of the network impedance at stage N, see fig. 11, is much more sensitive to interfacial effects than the real part. Hence we focus on $\mathrm{Im}\, Z_N$, whose frequency–dependence is shown in fig. 12. For $N = 4$, an "anomalous" regime can be identified, where a power–law

$$\mathrm{Im}\, Z_N \sim \omega^{-\eta} \tag{91}$$

with $\eta < 1$ holds over about three decades. As indicated before, equating the total interfacial admittance with the bulk admittance, determines one characteristic frequency ω_N^* satisfying $\omega_N^* C l_N = \sigma_b$ or, by equation (86),

$$x_N^* = l_N^{-1} = L_N^{-d_f} \tag{92}$$

Both for $\omega \ll \omega_N^*$ and $\omega \gg \sigma_b/C$, we have $\mathrm{Im}\, Z_N \sim \omega^{-1}$. These ω–dependencies, including (91), suggest the scaling forms

$$-\sigma_b \mathrm{Im}\, Z_N \sim \begin{cases} x_N^*/x & x \ll x_N^* \\ (x_N^*/x)^\eta & x_N^* \ll x \ll 1 \\ (x_N^*)^\eta/x & 1 \ll x \end{cases} \tag{93}$$

Actually, the ω–independent coefficients are fully determined by using $\mathrm{Im}\, Z_N \simeq (\omega C l_N)^{-1}$ for $\omega \ll \omega_N^*$, see our above discussion, and by requiring continuity at the two crossovers. So far, the exponent η remained undetermined. However, comparison with (85) for $x \gg 1$ and (90) fixes η. Since $-\sigma_b \mathrm{Im}\, Z_N \simeq x^{-1}(L_N)^{-\tau}$ and $(x_N^*)^{-1} = L_N^{d_f}$, we have $-\sigma_b \mathrm{Im}\, Z_N \simeq x^{-1}(x_N^*)^{\tau/d_f}$, which yields

$$\eta = \tau/d_f \tag{94}$$

This is the desired relationship between the dynamic exponent η and geometrical properties of the interface.

In most cases τ is near unity, so that $\eta \approx 1/d_f$. Nevertheless, deviations from this approximation are significant, as shown by H. Ruiz–Estrada et al. [115]. The reason is that merely by the fractal dimension d_f one does not distinguish between protrusions and pores which, however, influence the impedance in different ways. In particular, the ac–impedance at higher frequencies is governed predominantly by the protrusions. Precisely this aspect is taken into account through the exponent τ.

The appearance of an exponent $\tau < 1$ in the scaling of the high–frequency impedance with the system size, see the last relation in (93), has been verified independently by numerical computations in Ref. [115] up to stage $N = 5$.

A fully analytical, albeit approximate approach has been devised within the frame of position–space renormalization. Employing that method is suggested by the hierarchical structure of the model in fig. 11. Results are consistent with (93). An extended version of the method is able to reproduce the numerical data quantitatively, see the full curves in fig. 12. This implies a reliable calculation of the exponent τ. Similar calculations, both numerical and by renormalization, were successfully applied to boundaries of the type of fig. 11 but with a certain degree of randomization [115].

The argument that leads to equation (94) in the case of a two–dimensional electrolyte–electrode system, can easily be generalized to an arbitrary embedding dimension d. If L denotes the system size (again for fixed smallest length scale taken as unity) then the bulk and the interfacial admittances scale as $\sigma_b L^{d-2}$ and $\sigma_i L^{d_f}$, respectively. Equating both quantities yields $x^* = \omega^* C/\sigma_b \sim L^{d-2-d_f}$, instead of (92). In the three frequency–regimes distinguished in (93) the (dimensionless) impedance $-\sigma_b \mathrm{Im}\, Z$ now takes the form L^{-d_f}/x for $x \ll x^*$; $(L^{-d_f}/x^*)(x^*/x)^\eta$ for $x^* \ll x \ll 1$ and $(L^{-d_f}/x^*) \cdot x^{*\eta}/x$ for $1 \ll x$. As before, the last expression must

be equal to $L^{-\tau}/x$. Thus we recover the result

$$\eta = \frac{\tau + 2 - d}{d_f + 2 - d} \tag{95}$$

which was proposed earlier [143] and tested experimentally [144].

Acknowledgments

Many of the concepts and results presented in this paper have been obtained in close collaboration with A. Bunde. We thank him for many stimulating discussions and ideas. We are furthermore grateful to our coworkers on various aspects of dispersive ion transport in complex systems: D. Knödler, P. Pendzig and T. Höhr for their extensive work on the counterion model including its NCL features, R. Blender and E. Roman for their work on percolation in composite ionic conductors, M. Meyer for his investigation of spin-lattice relaxation in systems with percolative disorder, B. Rinn for his studies on the EMA with site energy disorder and the NCL regime, M. Porto and F. Scheffler for their analysis of the scaling features of conductivity spectra in models with site energy disorder, and R. Blender and H. E. Roman for their work on disperse ionic conductors and fractal electrodes. For much detailed information on experiments as well as critical discussions of theoretical concepts and results we should like to thank C. Cramer, K. Funke, P. Heitjans, M. D. Ingram, H. Jain, O. Kanert, K. L. Ngai, A. S. Nowick, and B. Roling.

References

[1] K. Funke, Progr. Solid State Chem. **22**, 111 (1993).

[2] C. A. Angell, K.L. Ngai, G.B. McKenna, P.F. McMillan, and S.W. Martin, J. Appl. Phys. **88**, 3113 (2000).

[3] W.K. Lee, J.F. Liu, and A.S. Nowick, Phys. Rev. Lett. **67**, 1559 (1991).

[4] A.S. Nowick, B.S. Lim, and A.V. Vaysleyb, J. Non–Cryst. Solids **172–174**, 1243 (1994).

[5] A. Pimenov, J. Ullrich, P. Lunkenheimer, A. Loidl, and C.H. Rüscher, Solid State Ionics **109**, 111 (1998).

[6] X. Lu, and H. Jain, J. Phys. Chem. Solids **55**, 1433 (1994).

[7] M. D. Ingram, in: *Material Science and Technologie*, Vol. 9, (VCH Verlagsgesellschaft, Weinheim 1991).

[8] P. Maass, J. Non–Cryst. Solids **255**, 35 (1999).

[9] A. K. Jonscher, Nature **267**, 673 (1977).

[10] A. K. Jonscher, *Dielectric Response in Solids* (Chelsea Dielectrics Press, London, 1983).

[11] O. Kanert, J. Steinert, H. Jain, and K.L. Ngai, J. Non–Cryst. Solids **131–133**, 1001 (1991).

[12] For a review, see J. Maier, Prog. Solid State Chem. **23**, 171 (1995).

[13] S. Indris, P. Heitjans, H.E. Roman, and A. Bunde, Phys. Rev. Lett. **84**, 2889 (2000).

[14] For a review, see B. Sapoval, in "Fractals in Disordered Systems", edited by A. Bunde and S. Havlin (Springer Verlag, Berlin, 1991) p. 207.

[15] D. P. Almond, G. K. Duncan, and A. R. West, Solid State Ionics **8**, 159 (1983); D. P. Almond, and A. R. West Solid State Ionics **9/10**, 277 (1983).

[16] J. L. Barton, Verres Réfr. **20**, 328 (1966).

[17] T. Nakajima, in *Annual Report, Conference on Electic Insulation and Dielectric Phenomena* (National Academy of Sciences, Washington DC, 1972), p. 168.

[18] H. Namikawa, J. Non–Cryst. Solids **18**, 173 (1975).

[19] B. Roling, A. Happe, K. Funke, and M. D. Ingram, Phys. Rev. Lett. **78**, 2160 (1997); in this work the BNN relation was not used to scale the spectra but the authors used $\omega_\sigma \propto \sigma_{\rm dc}T/n$, which corresponds the BNN crossover frequency if $\Delta\epsilon$ follows a Curie law, $\Delta\epsilon \propto n/T$.

[20] D. L. Sidebottom, Phys. Rev. Lett. **82**, 3653 (1999).

[21] D. L. Sidebottom, B. Roling, and K. Funke, Phys. Rev. B **63** 024301 (2001).

[22] T. B. Schrøder, and J. C. Dyre, Phys. Rev. Lett. **84**, 310 (2000).

[23] R. Kohlrausch, Ann. Phys. Lpz. **12**, 393 (1847); Pogg. Ann. Phys. **91**, 179 (1854).

[24] G. Williams, and D. C. Watts, Trans. Faraday Soc. **66**, 80 (1970).

[25] F. Alvarez, A. Alegnia, and J. Colmonero, Phys. Rev. B **44**, 7306 (1991).

[26] K. S. Cole, and R. H. Cole, J. Chem. Phys. **9**, 341 (1941).

[27] D. W. Davidson, and R. H. Cole, J. Chem. Phys. **19**, 1484 (1951).

[28] S. Havriliak, and S. Negami, J. Polym. Sci. **14**, 99 (1966).

[29] J. P. Bouchaud, and A. Georges, Phys. Rep. **195**, 128 (1990).

[30] We will use the symbol "$\sim$" in the sense of "asymptotic equal up to a constant", i.e. $\psi_\Gamma(\Gamma) \sim \Gamma^{-1-\beta_{\rm KWW}}$ for $\Gamma \to \infty$ means $\lim_{\Gamma\to\infty} \psi_\Gamma(\Gamma)/\Gamma^{-1-\beta_{\rm KWW}} = const.$

[31] E. W. Montroll, and G. H. Weiss, J. Math. Phys. **6**, 167 (1965).

[32] H. Scher, and M. Lax, Phys. Rev. B **7**, 4491 (1973).

[33] For the non-stationary CTRW, where the waiting time for the first jump of the particle is drawn from $\psi_\tau(\tau_1)$ rather than from $h(\tau_1)$, the value $\sigma = ne^2\langle l^2\rangle/6k_{\rm B}T\langle\tau\rangle$ corresponds to the dc–conductivity (stationary limit), while at high frequencies a limiting value $\sigma_\infty = ne^2\langle l^2\rangle\psi(0)/6k_{\rm B}T$ is obtained (as long as $\psi(0) \neq 0$).

[34] J. K. E. Tunaley, Phys. Rev. Lett. **33**, 1037 (1974).

[35] J. W. Haus, and K. W. Kehr, Phys. Rep. **150**, 263 (1987).

[36] D. A. G. Bruggemann, Ann. Phys. (Leipzig) **24**, 636 (1937).

[37] S. Kirkpatrick, Rev. Mod. Phys. **45**, 574 (1973).

[38] P. Soven, Phys. Rev. **156**, 809 (1967).

[39] V. V. Bryksin, Sov. Phys. Solid State **22**, 1421 (1980).

[40] B. Movaghar, B. Pohlmann, and G. W. Sauer, *Phys. Status Solidi* B **97**, 533 (1980).

[41] S. Summerfield, Solid State Commun. **39**, 401 (1981).

[42] T. Odagaki, and M. Lax, Phys. Rev. B **24**, 5284 (1981).

[43] I. Webman, Phys. Rev. Lett. **47**, 1496 (1981).

[44] B. I. Shklovskii, and A. L. Efros, *Electron Properties of Doped Semiconductors* (Springer Verlag, Heidelberg, 1984).

[45] A. Bunde, and S. Havlin, in *Fractals and Disordered Systems*, edited by A. Bunde and S. Havlin, 2nd ed. (Springer, Berlin, 1996).

[46] J. C. Dyre, and T. B. Schrøder, Phys. Rev. B **54**, 14884 (1996).

[47] J. C. Dyre, and T. B. Schrøder, Rev. Mod. Phys. **72**, 873 (2000).

[48] A. Bunde, J. Dräger, and M. Porto, in *Computational Physics*, edited by K. H. Hoffmann and M. Schreiber (Springer Verlag, Berlin, 1996).

[49] H. Böttger, and V. V. Bryksin, *Hopping Conduction in Solids* (VCH Verlag, Berlin, 1989).

[50] B. Movaghar, and W. Schirmacher, J. Phys. C, **14**, 859 (1981).

[51] O. Bleibaum, H. Böttger, and V. V. Bryksin, Phys. Rev. B, **56**, 6698 (1997).

[52] T. Wichmann, and K. W. Kehr, J. Phys.: Condens. Matter **7**, 717 (1995).

[53] P. Maass, B. Rinn, and W. Schirmacher, Phil. Mag. B **79**, 1915 (1999).

[54] P. Maass, and B. Rinn, Phil. Mag. B **81**, 1249 (2001)

[55] B. Rinn, dissertation, University of Konstanz, 2001.

[56] M. Porto, P. Maass, M. Meyer, A. Bunde, and W. Dieterich, Phys. Rev. B **61**, 6057 (2000).

[57] A. Hunt, J. Non–Cryst. Solids, **160**, 183 (1993).

[58] A. Hunt, J. Phys.: Condensed Matter, **4**, 5371 (1992); J. Non–Cryst. Solids, **220**, 1 (1997).

[59] P. W. Anderson, B. I. Halperin, and C. Varma, Phil. Mag. **25**, 1 (1972).

[60] W. A. Phillips, J. low Temp. Phys. **7**, 351 (1972).

[61] M. Pollak, and G. E. Pike, Phys. Rev. Lett. **28**, 1449 (1972).

[62] K. S. Gilroy, and W. A. Phillips, Phil. Mag. B **43**, 735 (1981).

[63] X. Lu, and H. Jain, J. Phys. Chem. Solids **55**, 1433 (1994).

[64] S. H. Glarum, J. Chem. Phys. **33**, 639 (1960).

[65] P. Bordewijk, Chem. Phys. Lett. **32**, 592 (1975).

[66] There is an additional relaxation occurring instantaneously at time $t = 0$ that comes from the defects being initially inside the interaction spheres. This contibution may be subsumed in ϵ_∞ or it can be neglected for $R \ll n^{-1/3}$.

[67] S. R. Elliott, and A. P. Owens, Phil. Mag. B **60**, 777 (1989).

[68] J. Klafter, and A. Blumen, Chem. Phys. Lett. **119**, 377 (1985).

[69] J. Klafter, and M.F. Shlesinger, Proc. natl. Acad. Sci. USA **83**, 848 (1986).

[70] M.F. Shlesinger, E.W. Montroll, Proc. natl. Acad. Sci. USA, **81**, 1280 (1984).

[71] H. Sher, and E.W. Montroll, Phys. Rev. B **12**, 2455 (1975).

[72] K. L. Ngai, Comments Solid State Phys. **9**, 127, (1979); *ibid.* 141 (1979).

[73] K. L. Ngai, and R. W. Rendell, J. Non–Cryst. Solids **131**, 233 (1990).

[74] K. Y. Tsang, and K. L. Ngai, Phys. Rev. E **54**, R3067 (1996).

[75] K.L. Ngai, and K.Y. Tsang, Phys. Rev. E **60**, 4511 (1999).

[76] K.L. Ngai, G.N. Greaves, and C.T. Moynihan, Phys. Rev. Lett. **80**, 1018 (1998).

[77] K.L. Ngai, Phil. Mag. B **77**, 187 (1998).

[78] K. Funke, and I. Riess, Z. Phys. Chem. Neue Folge **140**, 217 (1984); K. Funke, *ibid.* **154**, 251 (1987).

[79] M.F. Shlesinger, Solid State Communications **32**, 1207 (1979).

[80] J.H. Davies, P.A. Lee, and T.M. Rice, Phys. Rev. B **29**, 4260 (1984).

[81] A correlated backward jump occurs because the energy barrier for the backward jump is smaller than for jumps to other sites. If all jump directions would be equivalent the correlated backward jump rate would be zero, while the (non–correlated) backward jump rate would equal the jump rates to the other sites.

[82] The velocity correlation function is a symmetric function of time, which means that the integration over the δ-function in (39) gives a factor 1/2.

[83] K. Funke, S. Brückner, C. Cramer, and D. Wilmer, Phys. Chem. and Chem. Phys. in press.

[84] R.A. Tahir–Kheli, and R.J. Elliott, Phys. Rev. B **27**, 844 (1983).

[85] R. Granek, and A. Nitzan, J. Chem. Phys. **92**, 1329 (1990); **93**, 5918 (1990).

[86] M. Silverberg, M.A. Ratner, R. Granek, and A. Nitzan, J. Chem. Phys. **93**, 3420 (1990).

[87] R. Hilfer, and R. Orbach, Chem. Phys. **128**, 275 (1988).

[88] R. Hilfer, and R. Orbach, in "Dynamical Processes in Condensed Molecular Systems", edited by J. Klafter, J. Jortner and A. Blumen (World Scientific, Singapore, 1989), p.175.

[89] S. Druger, and M.A. Ratner, Phys. Rev. B **38**, 12589 (1988).

[90] O. Dürr, T. Volz, W. Dieterich, and A. Nitzan, J. Chem. Phys., in press.

[91] A. Bunde, and W. Dieterich, Phys. Rev. B **31**, 6012 (1985).

[92] P. Maass, J. Petersen, A. Bunde, W. Dieterich, and H. E. Roman, Phys. Rev. Lett. **66**, 52 (1991).

[93] J. Petersen, and W. Dieterich, Phil. Mag. B **65**, 231 (1992).

[94] P. Maass, M. Meyer, and A. Bunde, Phys. Rev. B **51**, 8164 (1995).

[95] D. Knödler, P. Pendzig, and W. Dieterich, Solid State Ionics **86-88**, 29 (1996).

[96] P. Pendzig, and W. Dieterich, Solid State Ionics **105**, 209 (1998).

[97] A. Heuer, and J. Reinisch, preprint.

[98] The small fraction of isolated clusters not being connected to the spanning cluster is removed from the lattice.

[99] A. Abragam, *The Principles of Nuclear Magnetism* (Clarendon Press, Oxford, 1962).

[100] D. Wolf, *Spin-Temperature and Nuclear-Spin Relaxation in Matter* (Clarendon Press, Oxford, 1979).

[101] M. Meyer, P. Maass, and A. Bunde, Phys. Rev. Lett. **71** 573 (1993).

[102] J. Jäckle, L. Piche, W. Arnold, and S. Hunklinger, J. Non–Cryst. Solids **20**, 365 (1976).

[103] D. P. Almond, and A. R. West, Solid State Ionics **26**, 265 (1988).

[104] D. Knödler, O. Stiller, and W. Dieterich, Phil. Mag. B **71**, 661 (1995).

[105] G. Carini, M. Cutroni, M. Federico, G. Galli, and G. Tripodo, Phys. Rev. B **30**, 7219 (1984).

[106] C. H. Hsieh, and H. Jain, J. Non–Cryst. Solids **203**, 293 (1996).

[107] K. L. Ngai, J. Chem Phys. **110**, 10576 (1999).

[108] A. S. Nowick, Solid State Ionics **136-137**, 1307 (2000).

[109] H. Jain, Metals, Materials and Processes **11**, 317 (1999).

[110] A. S. Nowick, A. V. Vayslab, H. Jain, and X. Lu, Mat. Res. Soc. Symp. Proc. **411**, 99 (1996).

[111] U. T. Höchli, K. Knorr, and A. Loidl, Adv. Phys. **39**, 605 (1990).

[112] T. Höhr, P. Pendzig, W. Dieterich, and P. Maass, submitted to Phys. Chem. Chem. Phys.

[113] P. Pendzig, dissertation, University of Konstanz, 1997.

[114] The derivation of Maxwells' equations for continuous media from the microscopic Maxwell equations requires an averaging procedure over a length scale L_0. In practice, L_0 should be at least about 30 interatomic distances [see J.D. Jackson, "Classical Electrodynamics" (John Wiley & Sons, Inc., New York, 1975) ch. 4]. The mixtures we are considering are composed of homogeneous regions of a size larger than L_0.

[115] H. Ruiz–Estrada, R. Blender, and W. Dieterich, J. Phys.: Condens. Matter **6**, 10509 (1994).

[116] J. Fleig, and J. Maier, J. Electroceramics 1:1, 73 (1997).

[117] In composite systems, the high–frequency dielectric constant ϵ_∞ is position–dependent and hence in principle affects the overall conductance properties at arbitrary frequency. To account for that, it is convenient to incorporate $\epsilon_\infty(\vec{r})$ into $\hat{\sigma}(\vec{r},\omega)$.

[118] D. Stauffer, and A. Aharony, "Introduction to Percolation Theory" (Taylor & Francis, London, 1992).

[119] A. Bunde, and S. Havlin in "Fractals and Disordered Systems", edited by A. Bunde and S. Havlin (Springer Verlag, 1991), p. 51.

[120] P.N. Sen, C. Scala, and M.H. Cohen, Geophysics **46**, 781 (1981).

[121] O. Dürr, W. Dieterich, P. Maass, and A. Nitzan, J. Chem. Phys. (submitted).

[122] A.L. Efros, and B.I. Shklovskii, Phys. Stat. Sol. B **76**, 475 (1976).

[123] D. Stroud, and D.J. Bergmann, Phys. Rev. B **25**, 2061 (1982).

[124] J.P. Clerc, G. Giraud, J.M. Langier, and J.M. Luck, Advances in Physics **39**, 191 (1990).

[125] B. Derrida, and J. Vannimenus, J. Phys. A: Math. Gen. **15**, L557 (1982).

[126] S. Havlin, and D. Ben Avraham, Advances in Physics **36**, 695 (1987).

[127] R. Blender, and W. Dieterich, J. Phys. C: Solid State Phys. **20**, 6113 (1987).

[128] J.C. Dyre, Phys. Rev. B **48**, 12511 (1993).

[129] S. Tyc, and B.I. Halperin, Phys. Rev. B **39**, 877 (1989).

[130] C.C. Liang, J. Electrochem. Soc., **120**, 1289 (1973).

[131] J. Maier in: Superionic Solids and Electrolytes ed. by A.L. Laskar and S. Chandra (Academic Press, New York, 1989) p. 137.

[132] A. Bunde, W. Dieterich, and E. Roman, Phys. Rev. Lett., **55**, 5 (1985).

[133] H.E. Roman, A. Bunde, and W. Dieterich, Phys. Rev. B **64**, 35 (1986).

[134] R. Blender, and W. Dieterich, J. Phys. C, **20**, 6113 (1987).

[135] For a review, see A. Bunde, and W. Dieterich, J. of Electroceramics 5:2, 81 (2000).

[136] D. Avnir, R. Gutfraind, and D. Farin, in "Fractals in Science", edited by A. Bunde and S. Havlin (Springer Verlag, Berlin, 1994) p. 229.

[137] J.B. Bates, Y.T. Chu, and W.T. Stribling, Phys. Rev. Lett., **60**, 627 (1988).

[138] B. Sapoval, R. Gutfraind, P. Meakin, M. Keddam, and H. Takenouti, Phys. Rev. E **48**, 3333 (1993).

[139] R. Blender, W. Dieterich, T. Kirchhoff, and B. Sapoval, J. Phys. A: Math. Gen. **23**, 1225 (1990).

[140] T.C. Halsey, and M. Leibig, Phys. Rev. A **43**, 7087 (1991).

[141] C.M. Mari, and G. Dotelli, Solid State Ionics **136–137**, 1315 (2000).

[142] R. Blender, and W. Dieterich, Solid State Ionics **28-30**, 82 (1988).

[143] Th.C. Halsey, and Michael Leibig, Ann. Phys. **219**, 109 (1992).

[144] A.E. Larsen, D.G. Grier, and Th.C. Halsey, Phys. Rev. E **52**, R2161 (1995).

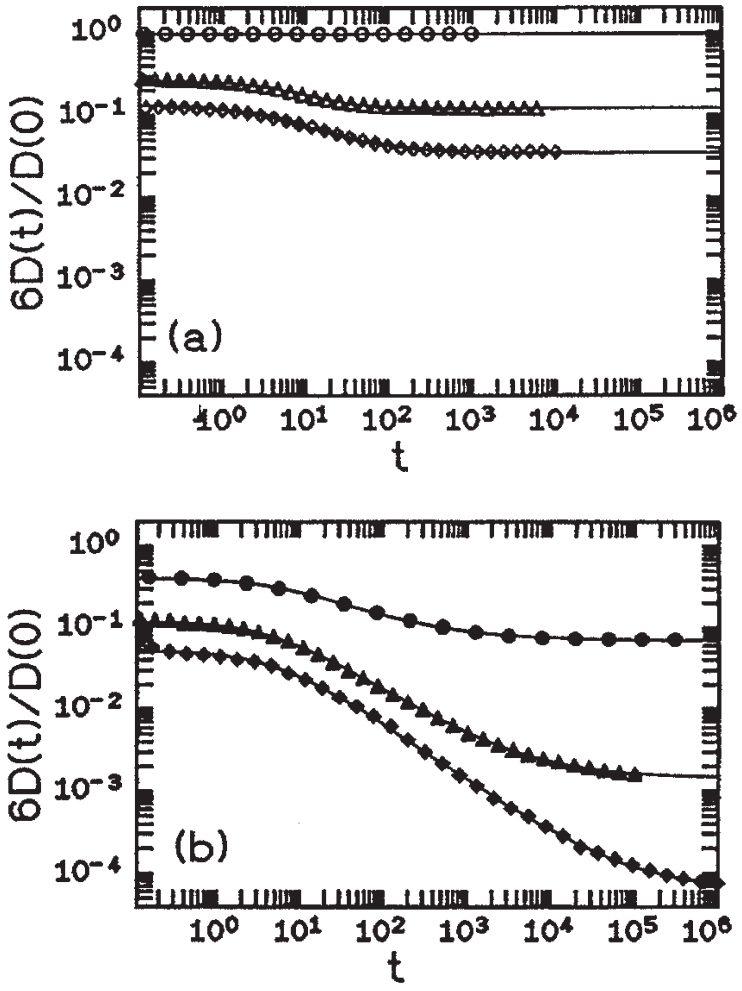

Fig. 1: Time–dependent diffusion coefficient of Coulomb lattice gas models with different plasma parameters Γ (redrawn from [94]. *(a)* Ordered lattice with $\Gamma = 0$ ($\circ$), 40 ($\triangle$), and 80 ($\Diamond$); *(b)* Percolative disorder, with a fraction $p = 0.4$ of accessible sites and $\Gamma = 0$ ($\bullet$), 40 ($\blacktriangle$), and 80 ($\blacklozenge$). Data points are from Monte–Carlo simulation and lines are fits according to eq. (46).

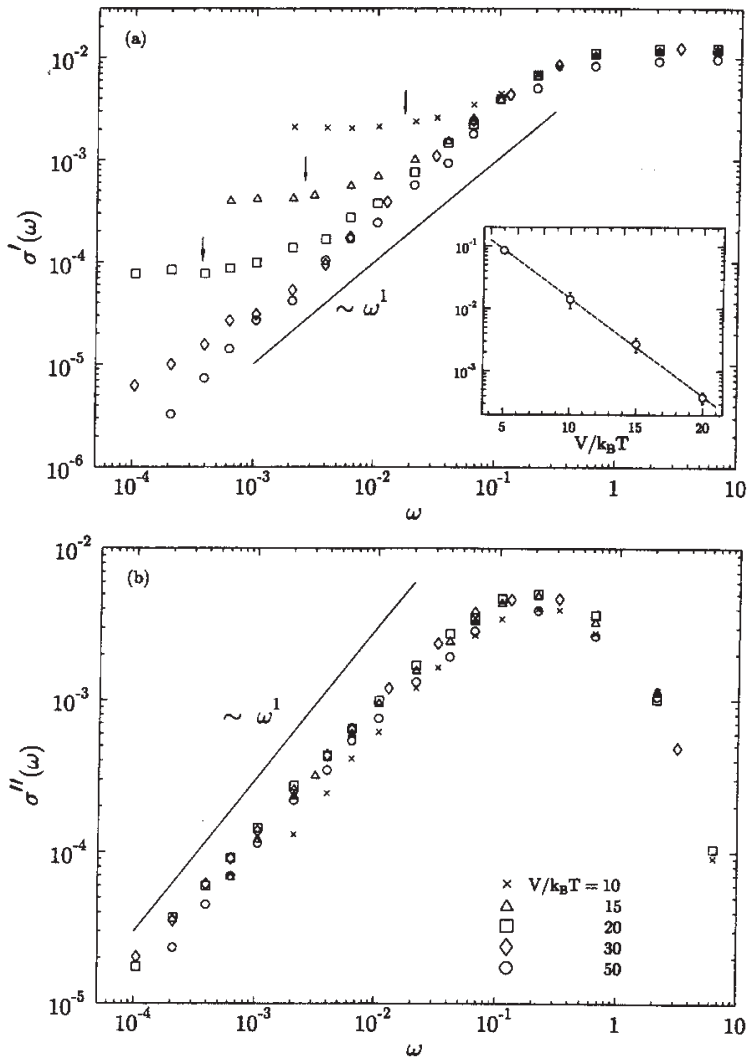

Fig. 2: Dynamic conductivity of the counterion model at a concentration $na^3 = 0.03$ of Coulomb traps for different temperatures (redrawn from [95]). *(a)* real part $\sigma'(\omega)$; *(b)* imaginary part $\sigma''(\omega)$. The straight lines have slope 1.

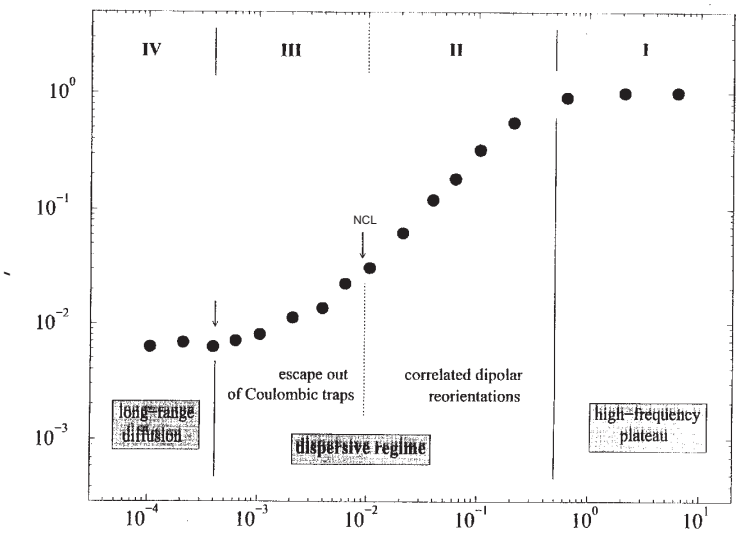

Fig. 3: Illustration of different frequency regimes in the dynamic conductivity of the counterion model at $na^3 = 0.03$ and $V/k_BT = 20$ (redrawn from [96]). The two intermediate regimes II and III pertain to "nearly constant loss" and Jonscher–type behavior, respectively.

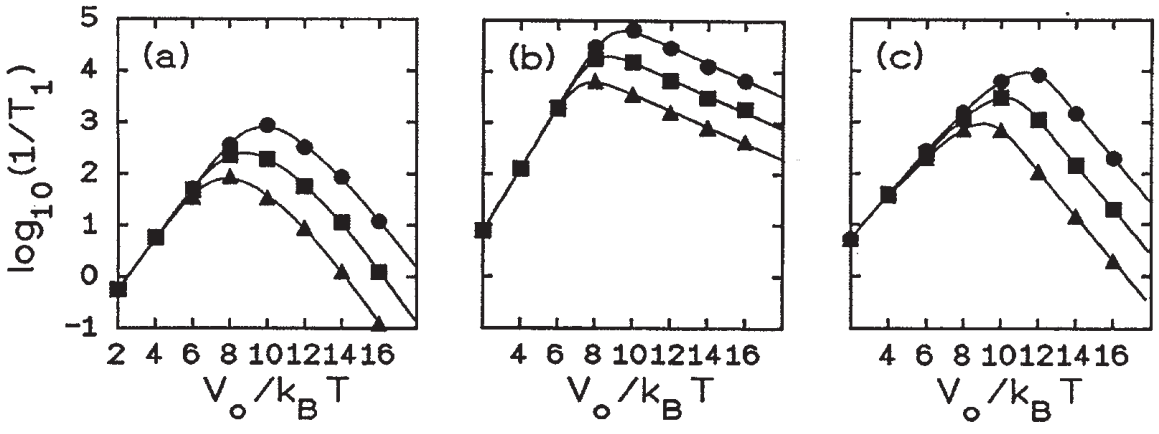

Fig. 4: Spin–lattice relaxation rate T_1^{-1} as a function of the inverse temperature (normalized quantities) of Coulomb lattice gas models (redrawn from [94]). *(a)* Ordered system, *(b)* highly correlated system ($\Gamma \gg 1$) with percolative disorder, *(c)* disordered system in the absence of Coulomb correlations ($\Gamma = 0$). Different symbols refer to different Larmor frequencies ω, covering one decade in each system. Details on the choice of parameters are found in ref. [94].

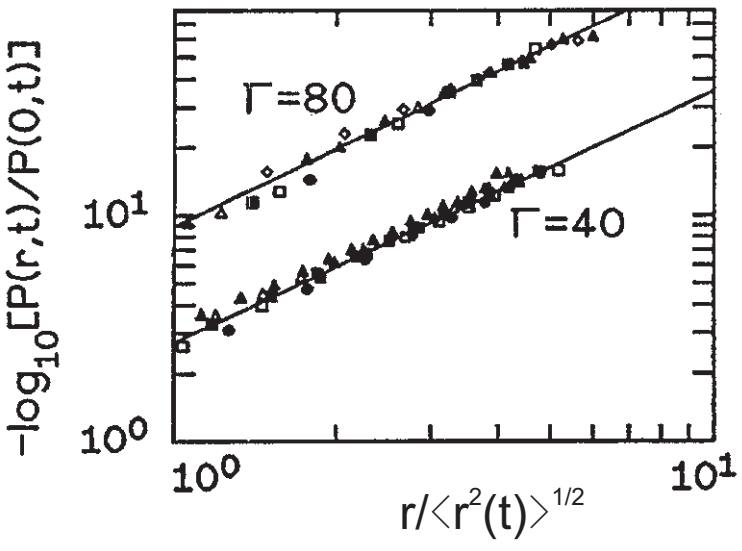

Fig. 5: Scaling plot of the distribution function $P(r,t)$ against $r/\langle r^2(t)\rangle$ in the disordered system. Different symbols refer to different times, covering about a factor 20 for $\Gamma = 40$ and a factor 70 for $\Gamma = 80$. Details are found in ref. [94].

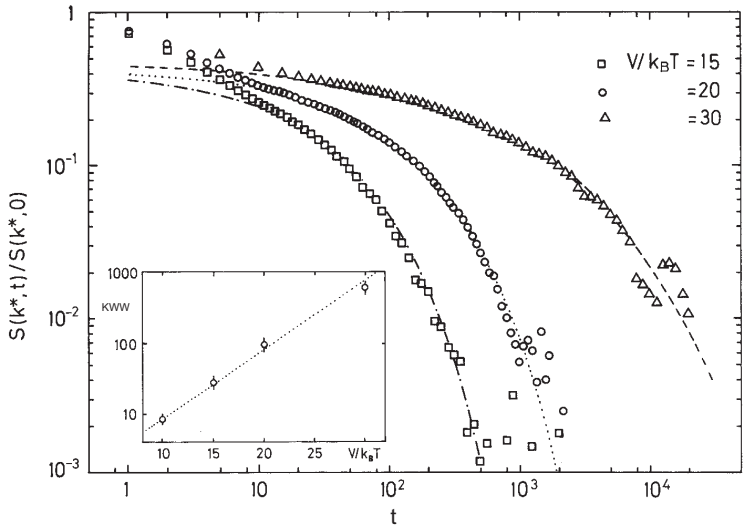

Fig. 6: Normalized relaxation function, see equation (68), determining the ultrasonic attenuation, computed for the counterion model for $na^3 = 0.03$ and different temperatures (redrawn from [104]). The inset shows an Arrhenius plot of the corresponding relaxation time τ_{KWW}.

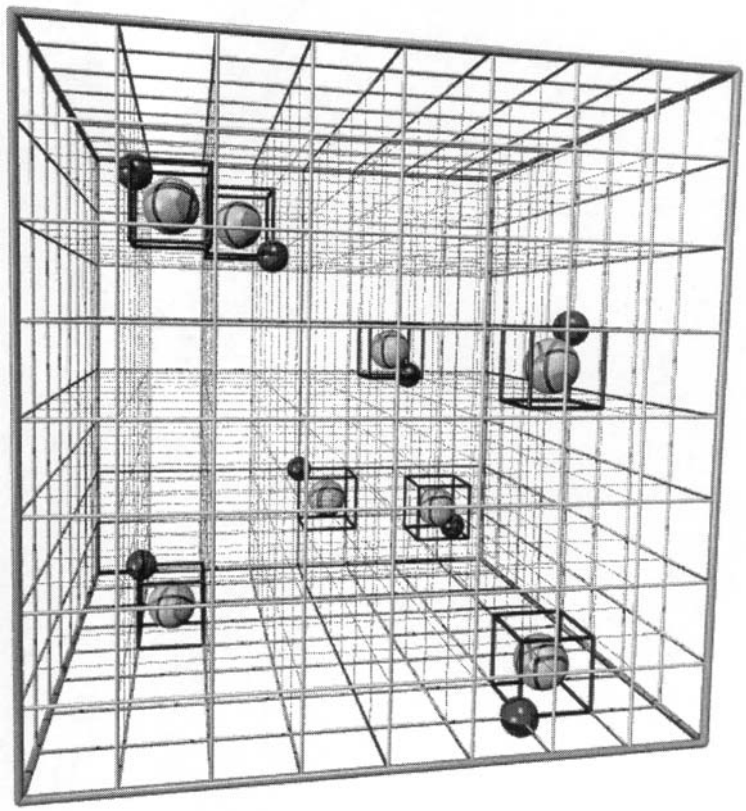

Fig. 7: Illustration of the dipolar lattice gas model with $na^3 = 1/64$.

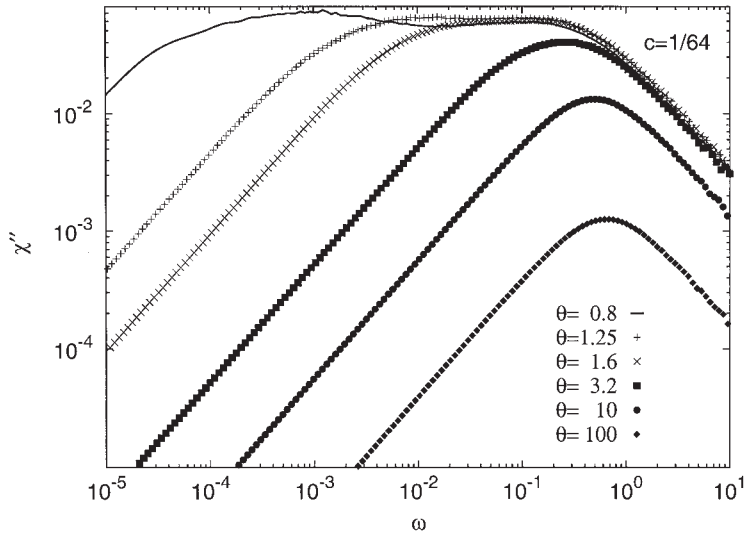

Fig. 8: Dielectric loss spectra of the dipolar lattice gas ($na^3 = 1/64$) at different temperatures.

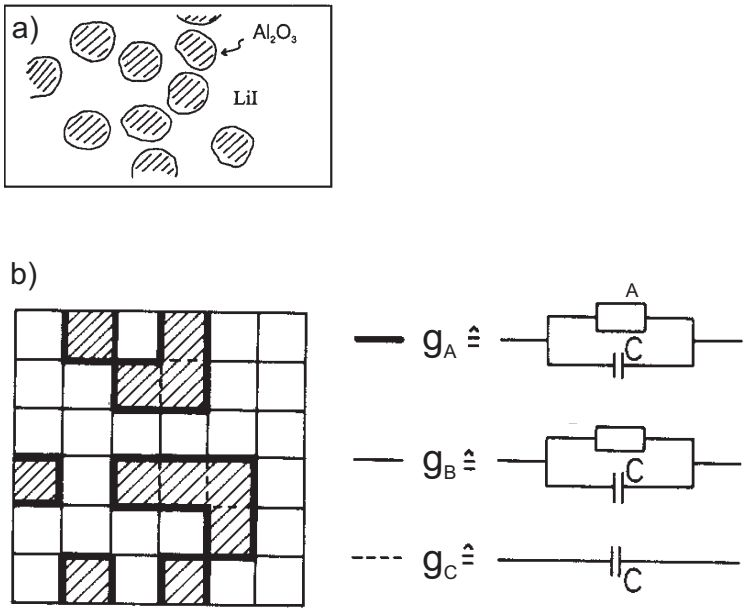

Fig. 9: *(a)* Schematic illustration of the microstructure in composite ionic conductors, exemplified by the LiI/Al_2O_3 system. *(b)* Section of an associated three–component random impedance network, displaying a highly conducting interface component (thick lines) that intervenes between normal conducting (unshaded) and insulating (shaded) regions.

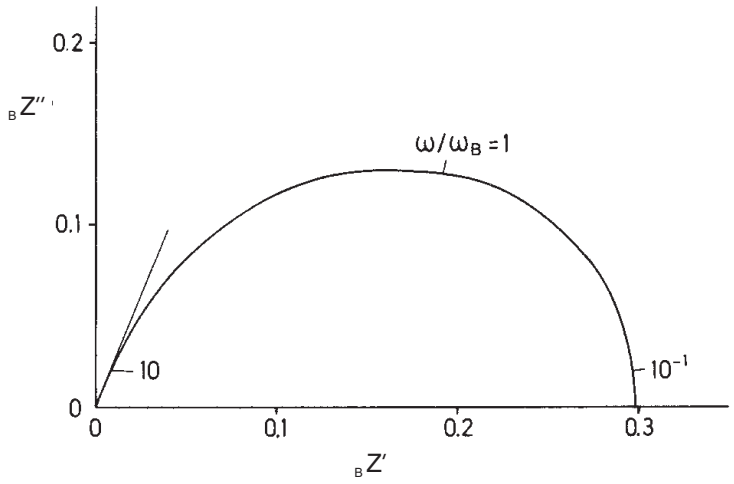

Fig. 10: Impedance diagram Z'' versus Z' for the network depicted in Fig. 9 at p_c' and $\tau = 10^2$ (redrawn from [142]). The straight line has slope $\tan\delta$.

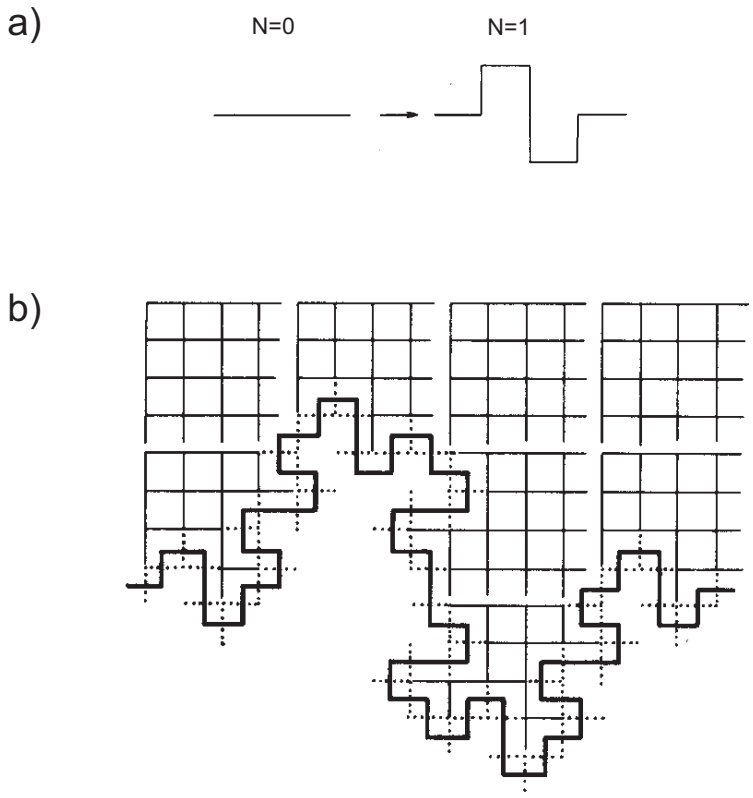

Fig. 11: *(a)* Generator of a quadratic Koch curve and *(b)* impedance network associated with a Koch–boundary at stage $N = 2$ between an electrolyte and an ideally blocking electrode. Within the electrolyte, network bonds have a real conductance σ_b, while interfacial bonds (dotted) have conductances $\sigma_i = -i\omega C$.

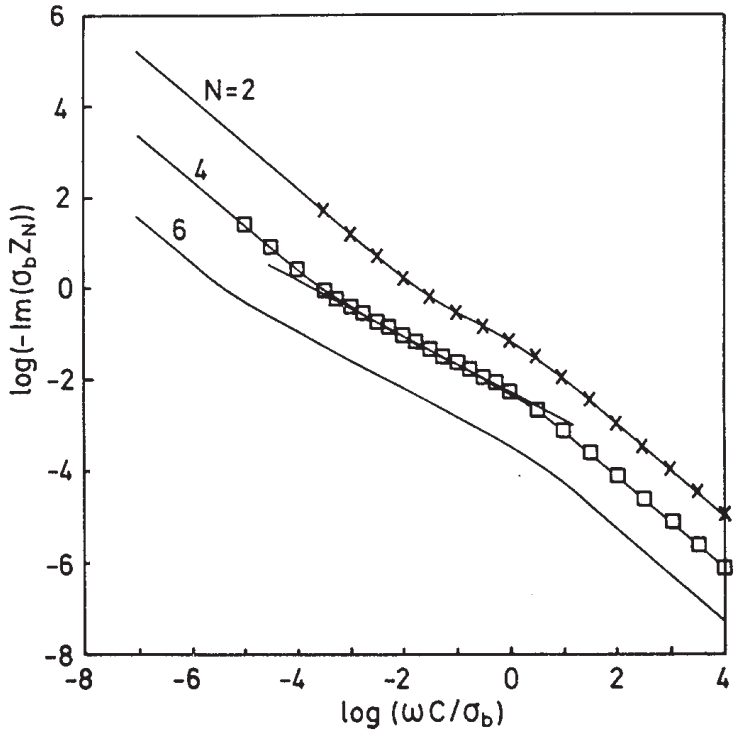

Fig. 12: Frequency–dependent imaginary part of the impedance in the model of Fig. 11 at increasing stages N. Full lines are from renormalization (redrawn from [115]). The straight line is a fit of numerical data for $N = 4$ in the anomalous regime and has slope $-\eta$, with $\eta \simeq 0.60$.